Degradation of fiber/matrix interface under various environmental and loading conditions: Insights from molecular simulations

Ruidong Wu[a,†], Xing Quan Wang[b,†], Danyang Zhao[b], Jia-ao Hou[a], Chao Wu[a,c]*, Denvid Lau[b]* and Lik-ho Tam[a]*

[a] School of Transportation Science and Engineering, Beihang University, 37 Xueyuan Road, Beijing 100191, China

[b] Department of Architecture and Civil Engineering, City University of Hong Kong, Hong Kong, China

[c] Department of Civil and Environmental Engineering, Imperial College London, South Kensington Campus, London SW7 2AZ, UK

[†] These authors contributed equally to this work

[*] Corresponding authors. E-mail: leo_tam@buaa.edu.cn (Lik-ho Tam); denvid.lau@cityu.edu.hk (Denvid Lau); wuchao@buaa.edu.cn (Chao Wu)

Abstract

Fiber-reinforced polymer composites have been increasingly applied as reinforcing and load-bearing components in building constructions and civil infrastructures. Long-term exposure to changing environmental and loading conditions leads to composite degradation, which is highly related to degraded structure and properties of interface and consequent interfacial debonding between fiber and matrix at nanoscale. By simulating interfacial structure and interactions with atomistic precision, molecular simulation allows a high fidelity to interfacial variations as affected by environmental and loading conditions. In this paper, molecular investigations of interfacial degradation between fiber and matrix under various environmental and loading conditions are reviewed. Model construction of interfaces formed by different fibers and matrixes and simulation of various environmental and loading conditions are firstly presented. Afterwards, mechanical and adhesion properties of molecular interfaces are introduced. Meanwhile, interfacial degradations under various environmental and loading conditions and underlying mechanisms are discussed. Further discussions on modeling and simulation of molecular interface are proposed for future researches. Overall, this work reviews previous molecular investigations of interfacial degradation of composites under different environmental and loading conditions, which contributes to evaluation of interfacial behaviors of composite materials.

Keywords: Fiber-reinforced polymer composites; Fiber/matrix interface; Environmental and loading conditions; Degradation; Molecular dynamics simulation

1. Introduction

During intended service life, building constructions and civil infrastructures are subjected to various environmental and loading conditions, which result in material degradation and increased risk of structural damage and failure. Thus, the reinforcement and strengthening of degraded structures has become a critical problem. Meanwhile, with stable development of society and economics, frequent population flow and transportation activities have placed increasing demand for improved load-bearing capacity and resilience of existing and new structures. Fiber-reinforced polymer (FRP) composites exhibit light weight, high stiffness- and strength-to-weight ratio, high fatigue resistance, and excellent customized properties. These exceptional mechanical properties are primarily originated from those of stiff and strong reinforcing fibers and good interfacial bonding between fiber and matrix, which largely ensures reinforcing efficiency of embedded fibers [1]. In past few years, several guidelines and design codes have been published to provide standard specifications for applications of FRP composites, including ASCE from United States in 2010, EUR27666 from Europe in 2016, and CECS from China in 2019 [2]. Accordingly, FRP composites have gained increasing applications as external reinforcements to strengthen degraded constructions and major load-bearing components in new structures, as shown in **Fig. 1(a)** [3, 4]. For instance, FRP laminates were used to strengthen concrete T-beam bridge in South Troy in the United States [5]; FRP wraps were used as reinforcements for damaged timber piles of railroad bridges in the United States [6]; pultruded FRP laminates were assembled into cable-stayed Fiberline bridge in Denmark [7]; and FRP members were assembled into seven three-meter-length FRP truss bridges at dock in China [8]. Furthermore, it is noted that applications of FRP composites could reduce the usage of traditional building materials including steel and concrete, which decreases the consumption of non-renewable materials and facilitates sustainable development of civil engineering [9].

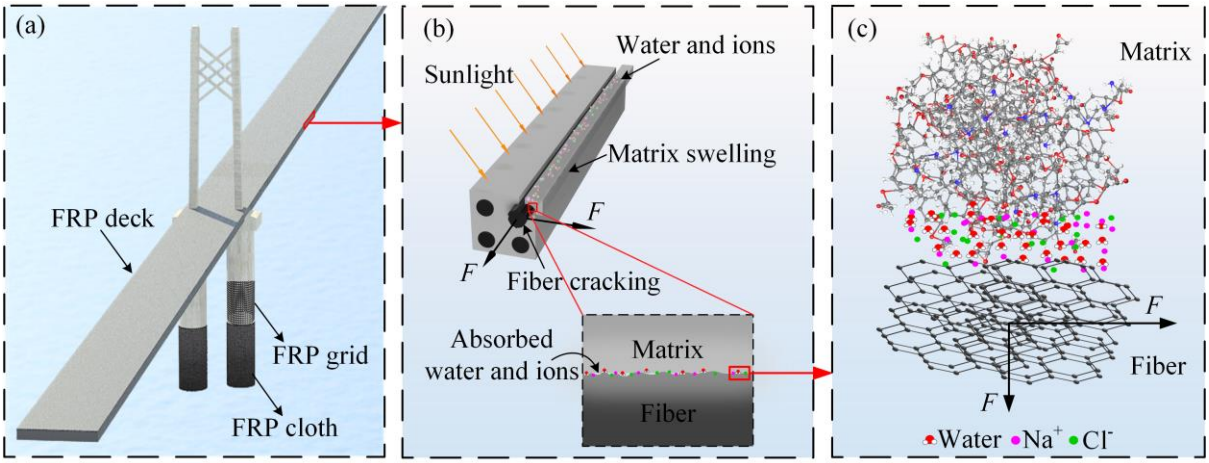


Fig. 1. Fiber-reinforced polymer (FRP) composite applications subjected to environmental and loading conditions: (a) structure, internal and external reinforcements made by composites; (b) external loads on composite are transferred through fiber/matrix interface, and water and salt ions diffuse into matrix and interface, which lead to matrix swelling, fiber cracking, and interfacial debonding, and degradation is accelerated at elevated temperature under sunlight; and (c) lead to structure and properties degradation of molecular interface at nanoscale.

For engineering applications, designed service life of building constructions and civil infrastructures is generally more than fifty years, during which structures and components made by FRP composite materials are inevitably subjected to various environmental and loading conditions, such as moisture, salt, high temperature (HT), sustained, impact, and cyclic loads. Structural and property degradations of FRP composites at structural, material, and fiber/matrix interface levels under various environmental and loading conditions have been reviewed in previous experimental studies [8, 10-14]. Specifically, long-term exposure to different environmental and loading conditions lead to significant weakening of matrix and overloading of certain regions of fiber. Accordingly, the stressed fiber is pulled out from the matrix and complete detachment occurs at the interface, as shown in **Fig. 1(b)**. Fiber pull-out and interfacial detachment facilitate crack propagation in composite, which leads to the reduction of mechanical properties and a brittle failure mode of composite materials in FRP structures. Although it is clear about the degradation and fracture behaviors of composite under

environmental and loading conditions, microscopic interfacial behavior during degradation process and its relationship with material failure are still not fully understood, which are required for ensuring long-term performance of composite materials.

Molecular dynamics simulation deals with molecular structure constructed from atoms as structural unit, which allows for accurate characterization of molecular interactions and precise control of environmental and loading conditions [15-18]. In molecular simulation, it starts from model construction of molecule with chemical composition and molecular structure according to experimental observations of investigated materials [19]. In molecular models, atoms interacts with neighboring atoms through bonded and non-bonded interactions, which are characterized by defining forcefield [19]. Afterwards, atom motion is determined based on Newton's second law, including displacement, velocity, and acceleration, which is integrated along with simulation time to simulate trajectory evolution of molecular models. After defining modeling and simulation details, the model is subjected to structural equilibration in different ensembles that impose stochastic impulsive forces on randomly selected atoms and control atom movement under thermostat and barostat, and reaches local minimum potential energy state where atom movement becomes stable, which is considered as equilibrated and stable structure of investigated material. Finally, the model is exposed to environmental and loading conditions for simultaneously observing microstructural changes and measuring properties of interest with time evolution. Therefore, molecular simulation is considered as a robust tool for investigating interfacial degradation and underlying mechanisms under influence of environment and loads [20].

This paper aims to provide in-depth understanding of degradation of fiber/matrix interface under environmental and loading conditions, by reviewing recent molecular simulation studies of fiber/matrix interface in wet, salt, elevated temperature environments coupled with various loading conditions. Firstly, the model construction of interfaces formed by fiber outer-layer

bonded with different matrixes, and the simulation of environmental and loading conditions are reviewed. Afterwards, mechanical and adhesion properties of different fiber/matrix interfaces are introduced. Moreover, degradations of fiber/matrix interfaces under different environmental and loading conditions are summarized, and underlying mechanisms are revealed. Finally, challenges and recommendations on modeling and simulation for future interfacial investigation are presented. This paper reviews recent molecular investigations on degradation of fiber/matrix interface under environmental and loading conditions, which provides fundamental insights into fiber/matrix interface degradation at a molecular level and forms basis of prediction of interfacial behaviors of FRP composite materials.

2. Modeling and simulation approach

In molecular simulation, the construction of molecular model is critical for precisely characterizing molecular structure and properties of interface in nature, which is firstly presented in this section, including fiber, matrix, and fiber/matrix interface. Afterwards, simulation details of various environmental and loading conditions are summarized. In order to simulate the fiber/matrix interface properly, accurate characterization of molecular interactions between fiber and matrix is required, which are defined in the applied forcefield, as presented at the end of this section.

2.1 Molecular modeling of fiber/matrix interface

In molecular simulations, local fiber/matrix interface at microscale as shown in **Fig. 1(b)** is commonly represented by a bilayer or sandwiched system composed of fiber and polymer matrix at nanoscale as shown in **Fig. 1(c)**. Among all the reinforcing fibers, glass fiber (GF) and carbon fiber (CF) have become the most widely used fibers in composite applications, due to their high stiffness and strength, good insulating property, and reasonable prices [21, 22].

For GF in the interfacial model, molecular structure of fiber outer layer is characterized by amorphous α-quartz silica, which is the main component of glass and is the configuration close to real GF surface, as shown in **Fig. 2(a)** [23, 24]. Atomistic model of silica unit cell is constructed from basic lattice parameters, which is repeated in x, y, and z direction to build crystalline silica model, and hydrogen atoms are used as termination atoms at upper and bottom surface of crystalline silica model [25]. During modeling process, amorphous silica is obtained through an annealing procedure of crystalline silica model [21]. Specifically, crystalline silica model is heated up to 5000 K at the rate of 1 $K \cdot ps^{-1}$ and equilibrated for 1 ns in canonical (NVT) ensemble, which is higher than the melting point of silica [26]. Afterwards, the model is quenched to 300 K at a constant cooling rate in isothermal-isobaric (NPT) ensemble at a constant pressure of 1 atm. The cooling rate ranges from 5 to 40 $K \cdot ps^{-1}$ in different simulations, which corresponds to rapid cooling process in experimental studies [27-29]. Finally, the system is further equilibrated at 300 K for 0.5 ns in NVT ensemble [21]. For the modeling of CF, according to experimental observation, nanometer-size graphite sheets preferentially align along the fiber axis and make up the graphite crystallite in fiber outer layer [30]. Accordingly, molecular structure of CF outer layer is represented by several parallel layers of graphite sheets, and the graphite sheets are terminated by hydrogen atoms in the two lateral dimensions, as shown in **Fig. 2(a)**. Compared with GF modeling, the construction of graphite sheets model does not require the annealing process [31-33]. In manufacturing process, fiber surface is generally coated with coupling agents including silane, epoxy, or emulsion coupling agents to create covalent bonds with the matrix so as to improve the handleability and compatibility between fiber and matrix [34]. In molecular simulation, tens to hundreds of molecules of silane coupling agent (SCA) are uniformly distributed on top of silica substrate representing GF outer layer, which form chemical bonds with silanol groups of hydroxylated silica surface to simulate treated GF surface [35, 36]. For the treatment of CF, similar number of molecules of epoxy

coupling agents are bonded to graphite sheets representing CF outer layer [37].

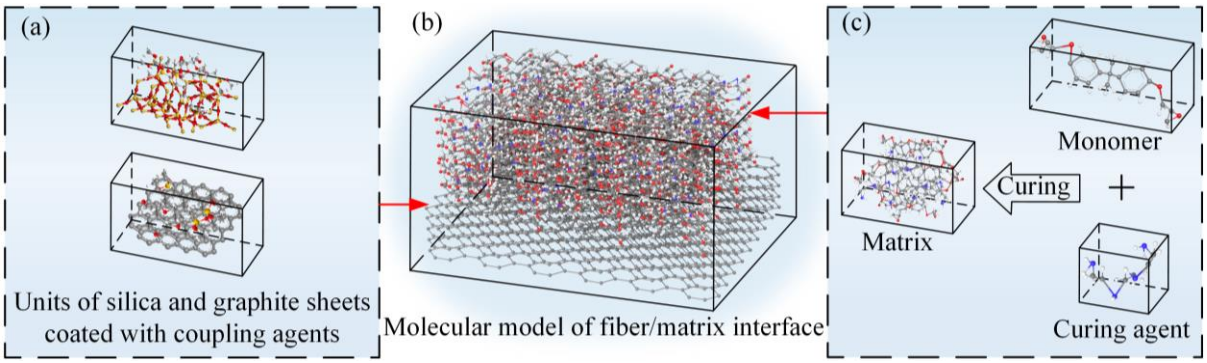


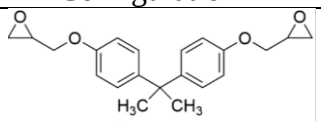
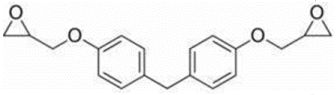
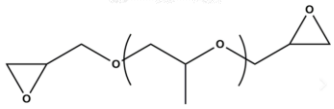
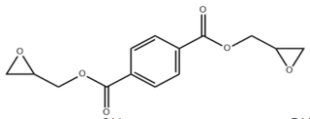
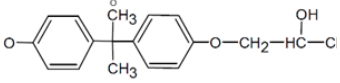
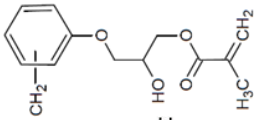
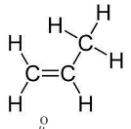
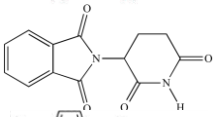
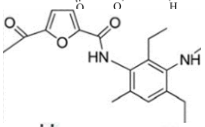
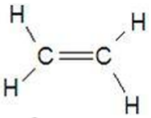
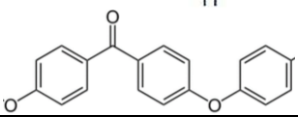
Fig. 2. (a) Fiber outer layer is replicated from the units of silica for glass fiber (GF) or several parallel graphite sheets for carbon fiber (CF) and coated with coupling agents as surface treatment, and (c) polymer matrix is constructed after polymerization process of monomer and curing agent, which are bonded together to form (b) the fiber/matrix interface, where CF/epoxy interface model is shown as a demonstration.

As another important component of FRP composite which binds, protects, and provides sufficient load-transfer with reinforcing fibers, matrix is expected to possess superior dimensional stability, excellent stiffness and strength, and stable chemical components, so as to facilitate its better combined properties with the fibers [38-40]. During the decades of research and manufacturing in the field of FRP composite, different types of polymers have been tested to be applicable candidates for matrix, which are mainly categorized into thermosetting and thermoplastic polymers [41, 42]. Notably, thermosetting polymer is a type of polymer consisting of cross-linked structure or heavily branched molecules, which cannot be processed repeatedly during polymerization process [43]. Specifically, epoxy resin is considered to be one of the most important high-performance thermosetting polymers, as it possesses better mechanical properties and durability, higher capability to resist moisture absorption and corrosive liquids compared with other thermosetting polymers [44]. According to different monomer types, epoxy could be divided into bisphenol-A epoxy, bisphenol-F epoxy, aliphatic glycidyl ether epoxy, and glycidyl ester epoxy, as shown in **Table 1**. Notably,

bisphenol-A epoxy is the mostly investigated epoxy in literatures, and diglycidyl ether of bisphenol-A (DGEBA) is the standard monomer. Meanwhile, DGEBA is usually cured by triethyltetramine (TETA) to form a cross-linked epoxy system, as shown in **Fig. 2(c)** [26, 45]. The first step of cross-linking process is to build a three-dimensional periodic molecular structure of epoxy monomers and curing agents. Afterwards, cross-linking process starts when potential reactive atoms of epoxy monomers and curing agent molecules located within current reaction radius are recognized [46]. After that, functional groups of epoxy monomers comprising those identified reactive atoms and reactive atoms of curing agents are open, and then the identified reactive atoms are connected to form cross-links by forming covalent bonds between reactive atoms [47]. Unreacted atoms of epoxy monomers and curing agent molecules are saturated with hydrogen atoms. Cross-linking process is generally carried out using the distance-based approach, where the reaction radius is normally set in the range of 0.3-1.0 nm, as there only form a limited number of cross-links at extended reaction radius over 1.0 nm [47-49]. With increasing reaction radius, cross-linking degree increases accordingly. Apart from the reaction radius, cross-linking density can be controlled by the proportion between monomers and curing agents, initial configuration, together with curing condition (e.g., temperature and pressure). Polymer matrices with different cross-linking densities possess various mechanical and thermodynamic properties. Generally, the modeled epoxy system possesses cross-linking densities consistent with experimental observations and the simulated epoxy properties are validated by comparing with available experimental data. Apart from epoxy resin, the commonly used thermosetting polymer matrixes include vinyl ester (VE) resin [50]. Similarly, VE resin includes bisphenol-A epoxy VE and novolac epoxy-based VE, where bisphenol-A-based dimethacrylate and novolac-epoxy are the standard monomers respectively, as shown in **Table 1**. Cross-linking process of VE is similar to epoxy matrix, where VE

monomers and reactive atoms of curing agents are connected by covalent bonds to form cross-links [50].

Table 1 Standard monomers and configurations of different types of polymers.

Type	Polymer	Standard monomer	Configuration
Thermosetting polymer	Epoxy	Diglycidyl ether of bisphenol-A (DGEBA)	
		Diglycidyl ether of bisphenol-F (DEGBF)	
		Poly (propylene glycol) diglycidyl ether (PPGDGE)	
		Diglycidyl terephthalate	
	Vinyl ester (VE)	Bisphenol-A-based dimethacrylate	
		Novolac-epoxy-based VE	
Thermoplastic polymer	Polypropylene (PP)	Propylene	
	Polyimide (PI)	Imide	
	Polyamide (PA)	Amide	
	Polyethylene (PE)	Ethylene	
	Polyetheretherketone (PEEK)	Etheretherketone	

Apart from thermosetting polymer, thermoplastic polymer is another important type of matrix used in manufacturing process of FRP composite, which significantly differs from thermosetting polymer due to distinct chemical characteristics resulted from linear molecular structure that softens under heating and hardens under cooling [51]. Specifically,

polypropylene (PP) is the most widely utilized thermoplastic polymer matrix with good mechanical properties and low processing temperature, and the standard monomer and configuration of PP are listed in **Table 1**. PP molecular model is constructed by randomly packing PP chains in a simulation box, which is heated to 1000 K and equilibrated for 50 ps in NVT ensemble, and then quenched from 1000 to 300 K at a cooling rate of 10 $K \cdot ps^{-1}$ at 1 atm in NPT ensemble to achieve the targeted properties [16]. Other thermoplastic matrixes simulated in previous simulation investigations include polyimide (PI), polyamide (PA), polyethylene (PE), and polyetheretherketone (PEEK), and the standard monomers and configurations of different types of thermoplastic polymers are listed in **Table 1** [22, 52-54]. The modeling of these thermoplastic polymers is achieved by carrying out the annealing process similar to PP case above.

Based on the constructed molecular models of fiber and matrix, the models of fiber/matrix interface are developed. Specifically, the fiber/matrix interface is constructed by combing fiber and matrix model, and the CF/epoxy interface is shown in **Fig. 2(b)** as an example. In molecular simulation, the matrix is either placed on the top or bottom of fiber model to construct a bilayer interface model or placed both on the top and bottom of fiber model to construct a sandwiched interface system [31, 55]. Afterwards, different boundary conditions including periodic or non-periodic conditions are applied to the interface model [21, 56, 57]. Specifically, periodic boundary conditions are applied in all directions of the interface model to simulate the bulk infinite interface as that in real composite [21]. Comparatively, non-periodic boundary conditions are applied to model the interface model with a finite size, so as to avoid over-constraints on the interaction of local interface caused by periodic mirrored images [56, 57]. It is noted that Materials Studio and Packmol are most extensively used software for molecular modeling of fiber and matrix [58, 59].

2.2 Simulation of environmental and loading conditions

After appropriate setup of interface system, it is simulated under various environmental and loading conditions to investigate the effect of environmental and loading conditions on the degradation of interfacial properties. During long-term service life, FRP composite is subjected to various loads including tensile and shearing loads, and the load is transferred between fiber and matrix, which leads to the loading conditions at local interface in the form of constant velocity loads. Meanwhile, FRP composite is exposed to sustained loads by facilities or structure weight lasting for a long duration in reality, which leads to the relaxation behaviors of matrix and overloading of certain regions of fiber. With load transfer between fiber and matrix through fiber/matrix interface, interfacial sliding occurs, and interfacial creep leads to the increased regions of overloaded fibers and subsequent crack propagation and interfacial debonding [60]. Furthermore, the traffic or pedestrian movement on FRP composite results in changing loads on composite materials, which leads to cyclic loads at local interface, and further leads to the growth of microcracks in matrix and the stress concentration and debonding of the interface, as well as crack propagation along the interface [61]. For the loading configuration in bilayer interface system, the top or bottom region of interface is fixed and other region of interface is regarded as mobile part to reduce oscillation of atoms and allow for the adequate response of mobile part [56, 57]. For the sandwiched system, two different loading setups have been used, where the top and bottom regions of matrix are fixed as the boundary or subjected to external load, and the rest portion of the interface is considered as mobile part [62].

In the investigation on interfacial response under constant velocity loads, for bilayer system, the center of mobile part of interface is generally subjected to the load in perpendicular direction of interfacial bonded plane in peeling simulation, or the load parallel to interfacial bonded plane in shearing simulation. For the sandwiched system in peeling simulation, the top

and bottom regions are subjected to external load in perpendicular direction of interfacial bonded plane. Comparatively, in shearing simulation, the top and bottom regions of matrix are fixed, and the center of fiber is loaded parallel to interfacial bonded plane. In peeling case, the interface model is subjected to load at constant strain rates ranging from 10^6-10^{11} s^{-1} or pulling rates ranging from 2.5 to 40.0 $m \cdot s^{-1}$, while for shearing simulation, the interface is loaded at a constant velocity of 1.0 to 4.0 $m \cdot s^{-1}$, which have been extensively used to investigate interface under constant velocity loads [46, 52, 63-67]. To further determine the dependence of pulling rate on probing the molecular mechanics, the rate dependence is investigated by carrying out a set of interfacial separation simulations with varying pulling rates [55, 68]. It is reported that there is no noticeable change of force-displacement curves at pulling rates ranging from 0.5 to 5.0 $m \cdot s^{-1}$, while it could lead to discrepancies between theoretical end experimental results if a higher pulling rate over 10.0 $m \cdot s^{-1}$is selected. In order to capture proper interfacial deformation behavior and consider the computational cost, the rates under slow deformation regime from 0.5 to 5.0 $m \cdot s^{-1}$ are preferred to be selected in simulations. For simulating the fiber/matrix interface under sustained loads, the peeling and shearing loads are applied at a constant level with the loading configuration similar as constant velocity loading cases [56, 57]. Specifically, the interface is loaded at various levels of sustained loads, and the applied load levels are lower than the interfacial strength [56, 57]. At each load level, the displacement of mobile part is recorded and the microstructural configuration is captured. To simulate the fatigue response of interface, interfacial model is subjected to cyclic loads for certain cycles along directions perpendicular and parallel to interfacial bonded plane to simulate tensile and shearing loading cases respectively [37]. Cyclic load is simulated by applying the strain along the loading direction following sinusoidal function, where the initial strain, amplitude, and period are set as 5%, 0.5%, and 1 ps respectively, which have been used to simulate fatigue behaviors of CF/epoxy interface in previous studies [37, 69].

Various environmental conditions such as wet, salt and elevated temperature are simulated to investigate the effect of environment on interfacial structures and properties. Wet and marine environments in real applications lead to the absorption of water and salt ions and affect the composite structure and properties. During water absorption, the moisture content of composite material increases gradually at first, and then tends to stabilize after saturation [70]. For simulating water absorption in molecular simulations, the interface is immersed in the environment with a large number of water molecules, and water molecules are considered to be absorbed in the interface if the distance between the oxygen atom of water and the interface is less than defined distance limit [71]. Diffusion process of absorbed water molecule in the polymer matrix is characterized by examining mean-square-displacement (MSD) and residence times of water molecules denoting the time of water molecules at a certain position. The saturated moisture absorption of the interface is determined by performing Grand Canonical Monte Carlo (GCMC) simulation, which is conducted by generating coordinates and orientation of water molecules randomly, and total potential energy of system after inserting each water molecule into the interface is calculated to determine whether or not to accept the addition of water molecule until there are no further insertions, where the interface has reached saturated absorption condition [21]. However, there are still challenges of these simulation approaches to simulate moisture absorption process and saturated moisture absorption state as it requires larger number of atoms and a long simulation time. Comparatively, after knowing saturated moisture content, different numbers of water molecules are added into the fiber/epoxy interfacial region to simulate the absorption condition of certain moisture content up to maximum of 4.0 wt%, which is close to the results of experiments [21, 69, 72, 73]. Meanwhile, to mimic saturated water absorption condition, the interface system is immersed in the water box containing a large number of water molecules with the density of 1 $g \cdot cm^{-3}$ [64, 74]. For salt environment, the investigation of absorption and

diffusion process of saltwater is limited, and the major focus is on saltwater immersion condition. Accordingly, the interface is immersed into saltwater containing 3.5 or 5.0 wt% sodium (Na^+) and chloride (Cl^-) ions, which is within the concentration range of 3.0-10.0 wt% used to investigate the effect of salt environment in experiment [45, 64, 75, 76]. For elevated temperature environment, the interface systems are equilibrated at targeted temperature levels ranging from 300 to 400 K, which is close to the usually investigated temperature range of 23 to 80 °C in experimental researches [47, 55, 77, 78]. In previous molecular investigations, the main simulation software includes open source code Large-scale Atomic/Molecular Massively Parallel Simulator (LAMMPS), Chemistry at HARvard Macromolecular Mechanics (CHARMM), J-OCTA, Groningen Machine for Chemical Simulations (GROMACS), and Assist Model Building with Energy Minimization (AMBER) [79-83]. Meanwhile, the simulation trajectory is mainly visualized using software Visualization for Virtual Molecular Dynamics (VMD), Open Visualization Tool (OVITO), and Electronic and Structural Analysis (VESTA) [84-86].

2.3 Molecular interactions of fiber/matrix interface

In the interface model, the accuracy of simulating molecular interactions between fiber and matrix depends heavily on the choice of forcefield, which is used to describe bonded E_{bonded} and non-bonded $E_{\text{non-bonded}}$ interactions between particles in the molecular structure, as shown in Eq. (1),

$$\begin{aligned} E &= E_{\text{bonded}} + E_{\text{non-bonded}} \\ &= E_{\text{bond}} + E_{\text{angle}} + E_{\text{torsion}} + E_{\text{out-of-plane}} + E_{\text{vdW}} + E_{\text{coul}} \end{aligned} \tag{1}$$

where bonded interactions E_{bonded} characterize covalent interactions among bonded atoms, including functional terms of bond stretching E_{bond}, angle bending E_{angle}, dihedral angle torsion E_{torsion}, and improper out-of-plane $E_{\text{out-of-plane}}$, and non-bonded $E_{\text{non-bonded}}$ interactions

characterize weak and dispersive interactions among non-bonded atoms, including van de Waals (vdW) E_{vdW} and Coulombic E_{Coul} interactions. In molecular investigations of fiber/matrix interface, non-reactive forcefield and reactive forcefield have been used. In non-reactive forcefield, it includes the simple and efficient pair-wise force fields for simulating the interface, and the bonds between neighboring atoms are defined empirically, which can be stretched and twisted, but cannot be broken, and hence chemical reactions are not simulated. These non-reactive forcefields use explicitly defined bonds and empirically derived interatomic potentials to capture the system potential energy as a function of atomistic positions. In recent atomistic simulation studies of GF/matrix interface systems, the commonly employed forcefields include Consistent Valence Forcefield (CVFF) and Condensed-Phase Optimized Molecular Potentials for Atomistic Simulation Studies (COMPASS) forcefield, as shown in **Table 2** [45, 53]. Meanwhile, other applied forcefields are Chemistry at HARvard Macromolecular Mechanics (CHARMM), van Beest, Kramer and van Santen (BKS), and Amber forcefield [21, 26, 87]. In recent atomistic simulation studies of CF/matrix interface systems, the commonly employed forcefields include CVFF and COMPASS forcefields, and other applied forcefields include Dreiding forcefield, Merck Molecular Forcefield (MMFF), Optimized Potential for Liquid Simulations-All Atom (OPLS-AA) forcefield, and Polymer Consistent Forcefield (PCFF), as shown in **Table 3** [16, 22, 31, 52, 64, 72, 88]. More recently, reactive forcefield (ReaxFF) has been increasingly used in molecular investigation to simulate the interactions formed between the components by bond-order formalism, where the order is achieved by calculating the interatomic distance [35, 36]. The chemical bonding in ReaxFF is implicitly described without complex and expensive quantum mechanical calculation, and hence bond breaking and formation are simulated dynamically. To simulate chemical reactions, ReaxFF has been used in simulating GF-bonded interface properties, as shown in **Table 2**, including density, electric potential, melting and quenching stages of GF, and debonding

process between GF and matrix. Meanwhile, ReaxFF has been employed to simulate interface strength, heat of formation, packing energy, and shearing fracture of CF-bonded interface, as shown in **Table 3** [36, 72, 89].

The aforementioned investigations mainly focus on all-atomistic model at nanoscale, where the accessible time and length scales of the investigated model are limited. To address the consideration of the heterogeneity of composites, it is preferred to characterize structural features at larger length scales, such as fiber surface roughness. In order to simulate the large-scale model, it requires excessive computational resources using all-atomistic molecular simulations. Comparatively, coarse-grained (CG) modeling is applied to build representations of complex systems at extended length scales that allows for keeping main chemical and physical peculiarities. In CG modeling, groups of atoms are clustered into CG beads, which interact with each other according to a suitable forcefield that accounts for both bonded and non-bonded interactions, which are parameterized to reproduce structural, mechanical, and thermodynamic properties observed from experiments [90]. In CG simulation, OPLS United Atom (OPLS-UA) force field has been used to investigate interfacial structure and properties of CF/epoxy interface at the magnitude of tens of nanometer, including mass density, potential energy, and internal stress of local interface, as shown in **Table 3** [91].

When the interfacial model is conditioned in wet and salt environment, the interactions within the solution and between interface and solution require particular attention. Water molecules are commonly represented using SPC, TIP3P, and TIP4P water model, as shown in **Table 2 and 3**. SPC model represents water as a tri-atomic molecule with rigid bonds, and both the length of oxygen-hydrogen bonds and the angle between those bonds are fixed, which has been used to investigate the adhesion properties of GF/epoxy interface under saturated moisture condition [92]. TIP3P water model has one oxygen atom and two hydrogen atoms, and the bond lengths and angles formed by these atoms are kept constant using SHAKE

algorithm, which has been applied to investigate GF/epoxy and CF/epoxy interfaces under different moisture conditions [64]. TIP4P water model includes a virtual atom with a negative charge next to the oxygen atom, which is used to improve the electrostatic distribution around water molecules, and it has been employed to investigate the adhesion properties of CF/epoxy interface under saturated moisture condition [74, 93]. In the simulation of salt ions, parameters for Na^+ and Cl^- ions are taken from the model which interact properly with water molecules or from the calculation by optimizing potential functions to reproduce osmotic pressure data [64]. The interactions between interface and solution are described by vdW and electrostatic interactions. vdW interaction is characterized by Lennard-Jones potential, and the parameters between interface and solution are generally obtained using different combination rules, including geometric mean combination rule and arithmetic mean combination rule [64, 94]. Short-range electrostatic interaction is calculated by forcefield parameters and cutoff at a certain truncated distance over 1.0 nm, as the interaction energy is very small over this cutoff distance [46, 63, 64]. Meanwhile, long-range electrostatic interaction is generally treated using particle-particle-particle- mesh (PPPM) solver [45, 56, 57].

3. Interfacial behaviors and properties of fiber/matrix interface

After model construction and simulation setup, the equilibration and deformation of interface systems are conducted and the mechanical and adhesion properties of fiber/matrix interface models are obtained to understand interfacial structure and properties between fiber and matrix at nanoscale.

3.1 Mechanical properties

In order to measure mechanical behaviors and properties, the interface is subjected to different external loads, including constant velocity, sustained, and cyclic loads. During

peeling simulation under constant velocity loads, tensile stress-strain curve of CF/epoxy interface is obtained, as shown in **Fig. 3(a)**. It is noted that interfacial deformation shows four typical stages close to interfacial delamination of FRP composites [95]. During initial stage, the stress keeps increasing until reaching the peak denoted as State *A*, where matrix remains in a close contact with fiber, as shown in **Fig. 3(b)**. Afterwards, the stress decreases rapidly during second stage, as matrix starts to detach from fiber surface, as shown in State *B*. During third stage, the stress further decreases and only a portion of polymer chains are attached to fiber, as shown in State *C*. Finally, the stress decreases to zero, where matrix is completely detached from fiber with a smooth surface, as shown in State *D*. From the peak of stress-strain curves, tensile strength of GF/epoxy interface is measured as around 286.2 and 340 MPa, while tensile strength of GF/PP interface is 130 MPa respectively, as listed in **Table 2** [36, 63, 87]. The larger tensile strength of GF/epoxy interface indicates that epoxy matrix could form a stronger interface with GF than PP matrix. For bilayer CF/epoxy interface with epoxy on top of graphite sheets, tensile strength is obtained as around 187 MPa, as shown in **Table 3** [47]. In other studies of sandwiched CF/epoxy interface where graphite sheets are positioned in the middle of two epoxy layers, tensile deformation is applied on two ends of epoxy layers along perpendicular direction [69, 88, 96]. Tensile strength is measured as 295.4, 377.5, and 406.5 MPa respectively, as listed in **Table 3**, which are much larger than 187 MPa obtained from bilayer CF/epoxy interface system, as interfacial contact and constraint of sandwiched interface are stronger due to periodic boundary conditions along interfacial plane. Moreover, it is observed that tensile strength (286.2 and 340 MPa) of GF/epoxy interface is at the same magnitude as that of CF/epoxy interface ranging from 187 to 406.5 MPa, and the difference could be originated from different modeling and simulation setups, boundary conditions, and loading rates used in peeling simulations. For CF/epoxy interface, tensile strength is higher than experimental value up to 63 MPa, while it is within tensile strength of 171-450 MPa

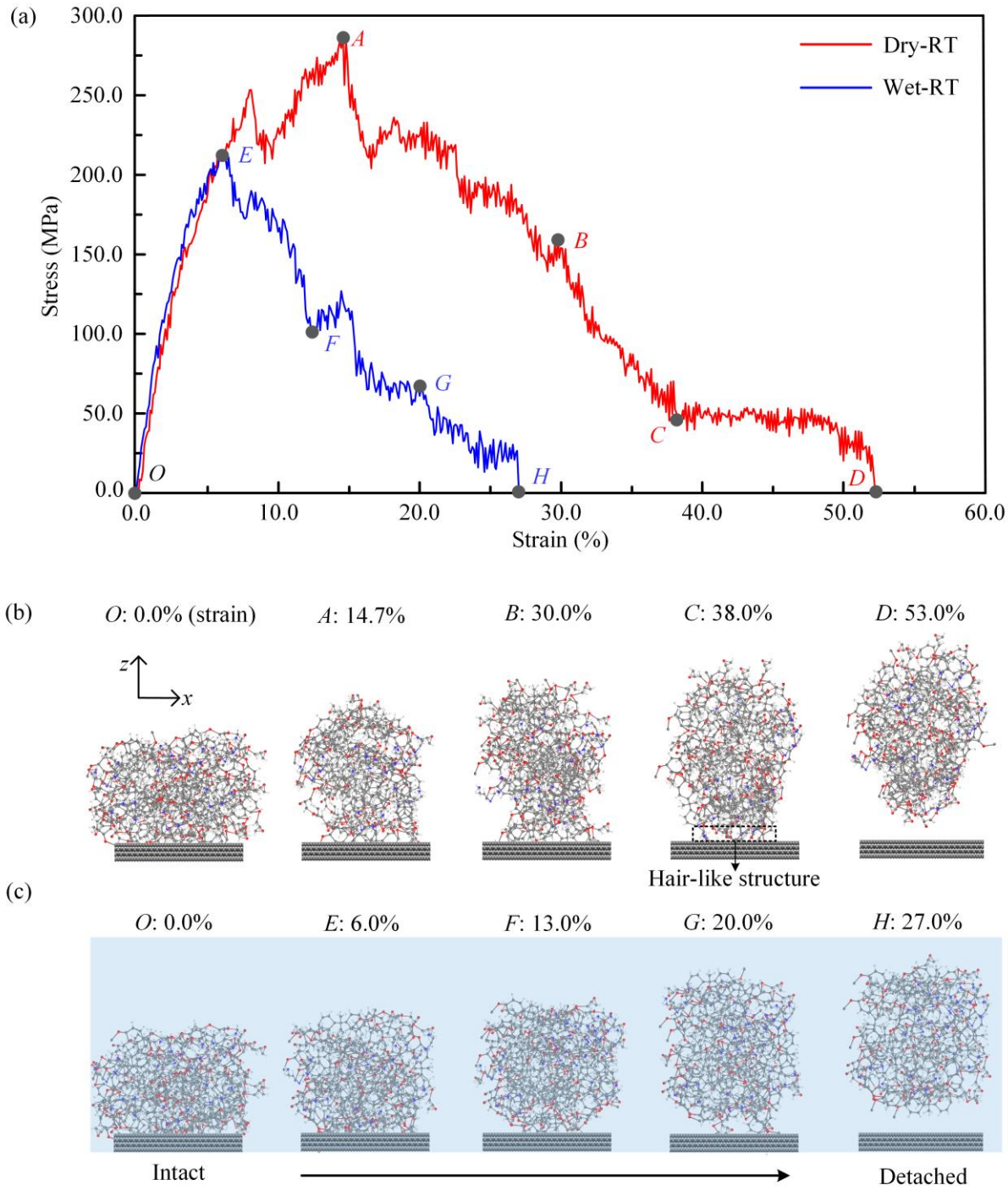


Fig. 3. (a) Stress-strain curves and (b, c) microstructural changes of CF/epoxy interface during peeling simulation at a constant velocity of 2.5 $m \cdot s^{-1}$ in (b) dry and (c) wet environments at room temperature (RT): four deformation stages are observed in dry environment, where the stress keeps increasing to the peak denoted as State *A* as interface remains intact, the stress decreases as interface starts to detach in State *B*; the stress further decreases as interface further detaches with a portion of polymer molecules forming the hair-like structure in State *C*, and stress decreases to zero as interface fully detaches in State *D*; while the interface shows similar

states from *E* to *H* in wet environment, where debonding process occurs faster with no obvious hair-like structure for impeding the debonding.

obtained from molecular simulations [47, 97, 98]. The overestimated tensile strength compared with experimental value is originated from higher pulling rate in molecular simulations, where the interface has shorter time for deformation and crack propagation. Furthermore, when silica surface is coated with SCA, tensile strength of GF/epoxy interface is improved significantly by up to 200%, as shown in **Table 2** [87], as SCA impedes interfacial detachment with mixed failure modes at interface and in matrix with residual polymer molecules at detached surface [87].

Shearing behavior of fiber/matrix interface is critical for understanding interfacial response under constant velocity loads. When fiber/matrix interface is subjected to constant velocity shearing loads, stress-strain curve is obtained, as shown in **Fig. 4(a)**. Accordingly, there is an initial stage where shear stress of intact interface increases rapidly, as denoted as State *A* in **Fig. 4(b)**, and second stage where the stress reaches plateau as interfacial sliding starts to occur steadily, as shown in State *B*. Subsequent two stages include third stage where the stress drops fast as the portion of matrix attached to fiber decreases, and final stage where the stress reaches zero as interfacial detachment occurs, which are not reported in shearing simulation as large planar surface is used to model fiber surface in interface system [55]. From maximum stress of curve, interfacial shear strength (IFSS) of GF/epoxy interface is 320 MPa as shown in **Table 2** [87]. For GF/PEEK interface, IFSS is measured as 40.3 MPa as shown in **Table 2**, which is close to experimental value of 45.2 MPa [53, 99]. For CF/matrix interface, IFSS of CF/epoxy and CF/PI interfaces is calculated as 188 MPa and 331.14 MPa respectively, as shown in **Table 3**, which are larger than experimental data of 24-139 MPa and 45-53 MPa [52, 72, 100, 101]. Compared with experiment, the simulation values are larger, which is resulted from higher pulling rates in molecular simulations similar as the overestimation of

tensile strength discussed previously. By incorporating SCA or functional groups on fiber surface, IFSS of GF/epoxy interface is improved significantly by up to 200% as shown in **Table 2**, which corresponds to tensile strength increment, as SCA addition leads to residual matrix attached to fiber surface after interfacial detachment [53, 87, 102].

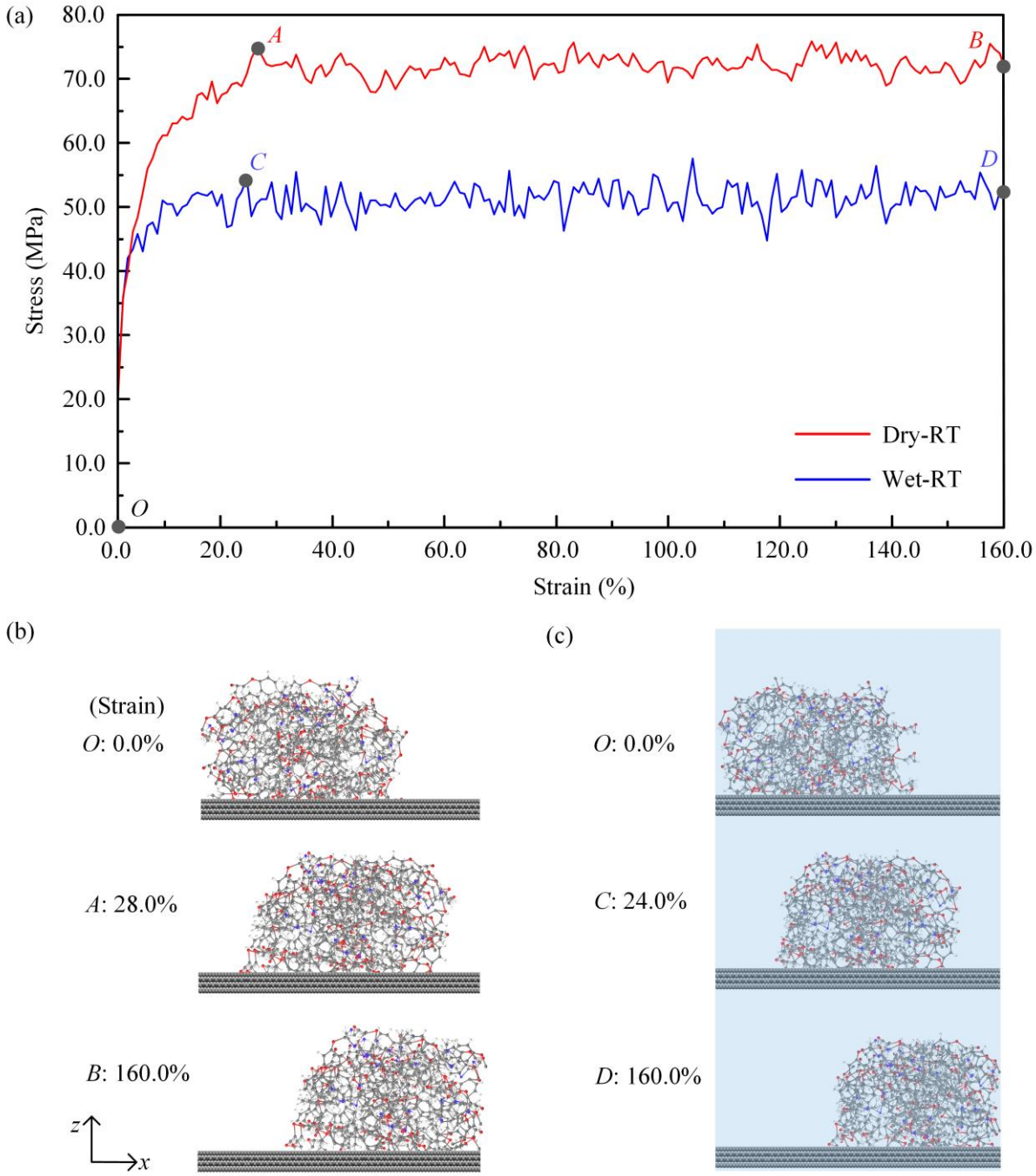


Fig. 4. (a) Stress-strain curves and (b, c) microstructural changes of CF/epoxy interface during shearing simulation at a constant velocity of 2.5 $m \cdot s^{-1}$ in (b) dry and (c) wet environments at

RT: two deformation stages are shown as a demonstration, including the initial stage where the stress increases rapidly as interface remains intact in State *A*(*C*), and the subsequent stage where the stress reaches the plateau as interfacial sliding starts to occur steadily in State *B*(*D*).

Apart from mechanical response under constant velocity loads, interfacial creep behaviors under sustained loads are of great concern for understanding interfacial degradation. When fiber/matrix interface is subjected to sustained tensile loads, strain-time curves measured at different load levels are shown in **Fig. 5(a)**. At low load levels, the strain increases gradually and reaches a constant level at the end of simulation timespan, while at high load levels, the strain increases significantly until detachment occurs, which are denoted as low and high load regime, respectively. Threshold stress between low and high load regime is obtained via dividing threshold force by interfacial contact area. For CF/epoxy interface, threshold stress is measured as 44.84-45.64 MPa, as shown in **Table 3** [103]. There is no experimental data for a direct comparison of threshold stress, while it is within the range of tensile strength up to 63 MPa obtained from experiment [97, 98]. Under low load regime below threshold load, the strain evolution presents three stages as shown in **Fig. 5(b)**, including an initial stage where the strain fluctuates around zero as interface remains closely intact with slight matrix elongation as denoted in State *A*, a subsequent stage where the strain increases slightly with an obvious matrix elongation in State *B*, and a final stage where the strain increase gradually slows down to reach a constant level as polymer deformation reaches a stable state in State *C* and *D* [103]. Under high load regime, the strain shows a much shorter fluctuation during initial stage compared with low load regime, as demonstrated in State *E* shown in **Fig. 5(c)**. Afterwards, the strain shows a faster increase during second stage where interfacial separation occurs gradually and matrix exhibits a larger elongation in State *F*, and a significant acceleration during final stage where interfacial separation accelerates in State *G*, until complete detachment in State *H*. Meanwhile, the transformation of strain energy and deconvolution of polymer

chains are also found to occur during creep [96].

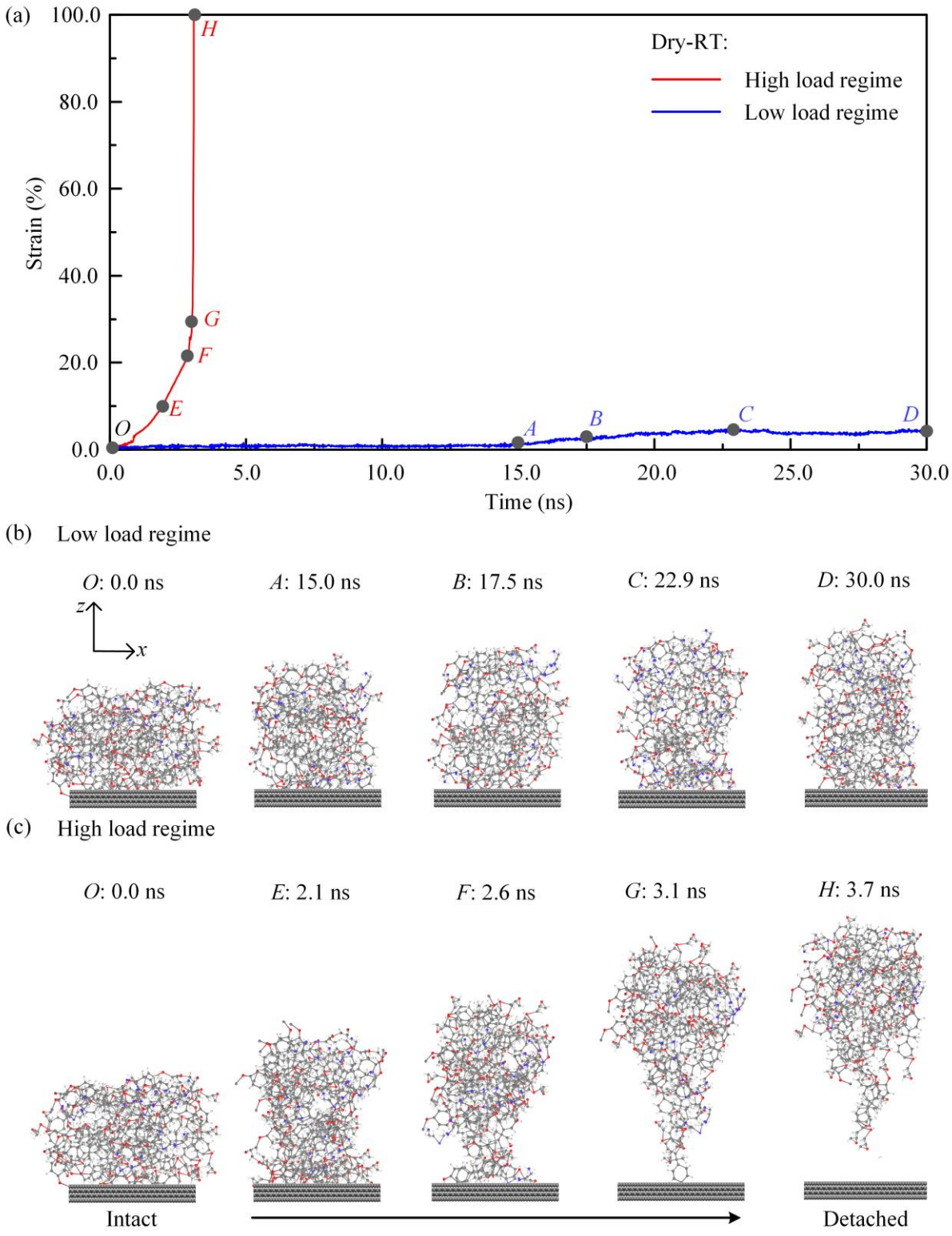


Fig. 5. (a) Strain-time curves and (b, c) microstructural changes of CF/epoxy interface under sustained peeling loads at 44.84 MPa (low load regime) and 48.04 MPa (high load regime) in

dry environment at RT: under low load regime, the interface exhibits three creep deformation stages including an initial stage where the strain fluctuates around zero as the interface remains closely intact in State *A*, a subsequent stage where the strain increases slightly with an obvious matrix elongation in State *B*, and a final stage where the strain reaches a constant level as the matrix deformation reaches a stable state in State *C* and *D*; under high load regime, the interface shows similar first and second stages with a larger matrix elongation in State *E* and *F*, while during third stage, the strain increases at a larger rate as interfacial separation accelerates in State *G*, until complete detachment in State *H*.

Interfacial creep behaviors under sustained shearing loads are important for the comprehensive understanding of interfacial creep response. During shearing creep of CF/epoxy interface, the strain evolution exhibits different responses under low and high regimes, which is similar as peeling creep case [56, 57]. For CF/epoxy interface, threshold stress between low and high load regime is measured as 28.02-28.82 MPa, as shown in **Table 3** [56, 57]. Threshold stress is slightly larger than that obtained through interfacial shearing creep using nano-indentation (24 MPa), which could be originated from structural voids and water absorption in experimental samples that lead to reduced interfacial strength [104]. By comparing with peeling creep case, threshold stress obtained from shearing creep is smaller, which demonstrates weaker resistance to creep along shearing direction. Under low load regime, the strain evolution exhibits a similar three-stage response as peeling creep case, as shown in **Fig. 6(a)**. During first stage, the strain shows an initial increase as slight interfacial sliding and matrix compression occur as denoted as State *A* in **Fig. 6(b)**, and increases slower during second stage as interfacial sliding and matrix compression slow down in State *B*. During third stage, the strain gradually reaches a constant level as interfacial sliding becomes stable in State *C* and *D* [56, 57]. Under high load regime, the strain increases faster during first two stages, as interfacial sliding occurs faster compared with low load regime in State *E* and *F* as shown in **Fig. 6(c)**, and significantly accelerates during third stage as interfacial sliding

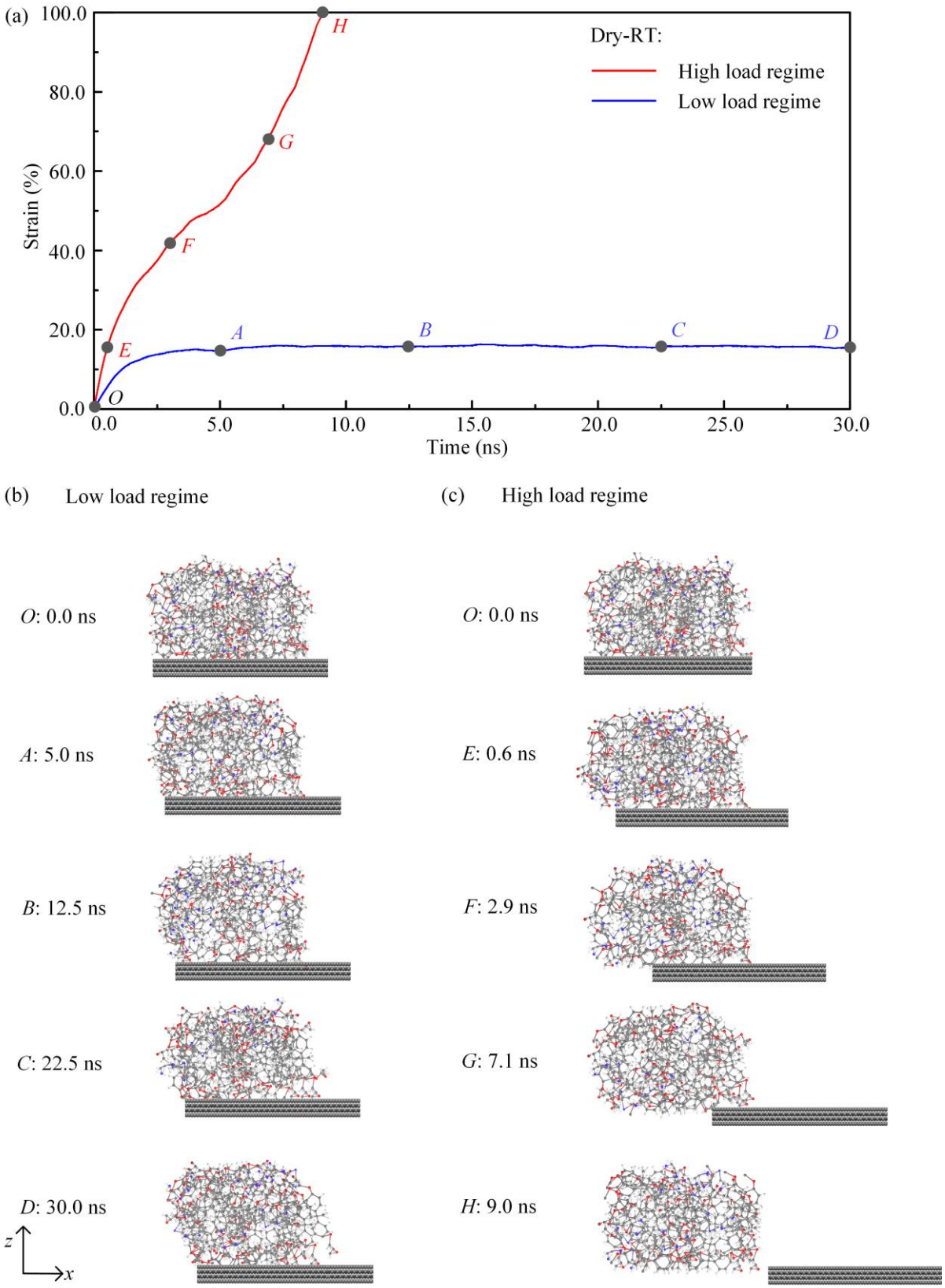


Fig. 6. (a) Strain-time curves and (b, c) microstructural changes of CF/epoxy interface under sustained shearing loads at 25.62 MPa (low load regime) and 28.82 MPa (high load regime) in dry environment at RT: under low load regime, the interface exhibits three creep deformation

stages including an initial stage where the strain shows an initial increase as a slight interfacial sliding and matrix compression occur in State *A*, a second stage where the strain increases slower as interfacial sliding slows down in State *B*, and the third stage where the strain reaches a constant level as interfacial sliding reaches a stable state in State *C* and *D*; under high load regime, the interface shows similar first and second stages in State *E* and *F*, and a different third stage as the strain increases significantly faster as interfacial sliding accelerates in State *G*, until final detachment in State *H*.

accelerates in State *G*, until final detachment occurs in State *H* [56, 57]. By comparing peeling and shearing creep cases, interfacial creep deformation and detachment are delayed in peeling case, as interface dissipates energy mainly through larger matrix elongation in peeling case, while mainly through interfacial deformation in shearing case.

Interfacial behaviors under dynamic loads require special consideration as dynamic loads are critical for crack growth at fiber/matrix interface and lead to interfacial degradation. For CF/epoxy interface under cyclic loads, mean stress-cycle number (*S*-*N*) curve is measured to characterize stress transfer of interface. Specifically, stress evolution of interface along loading direction is recorded during simulation, and maximum and minimum stress during each cycle is averaged as mean stress *S*, as shown in **Fig. 7**. From *S*-*N* curve under transverse cyclic loads perpendicular to fiber direction, mean stress *S* of interface keeps decreasing in initial several cycles, and then the decreasing becomes gradually slower at larger cycles [37, 69]. The decreasing mean stress *S* is resulted from the tendency of matrix molecular fragments to align along loading direction, which reduces close contact between fiber and matrix and inhibits interfacial stress transfer, leading to interfacial degradation. Specifically, initial mean stress of CF/epoxy interface is measured as 241.7 MPa, which reduces by 34% after 300 loading cycles under transverse cyclic loads [37]. Comparatively, under axial cyclic loads parallel to fiber direction, mean stress *S* shows a similar decreasing trend with increasing cycle number, while the decrease is much slower than transverse case, with only a reduction of 0.6% compared with

initial stress level after 300 loading cycles. The decrease of mean stress is much faster under transverse cyclic loads compared with axial case, which indicates larger interfacial resistance to cyclic loads along fiber direction due to stronger load carrying ability of fiber.

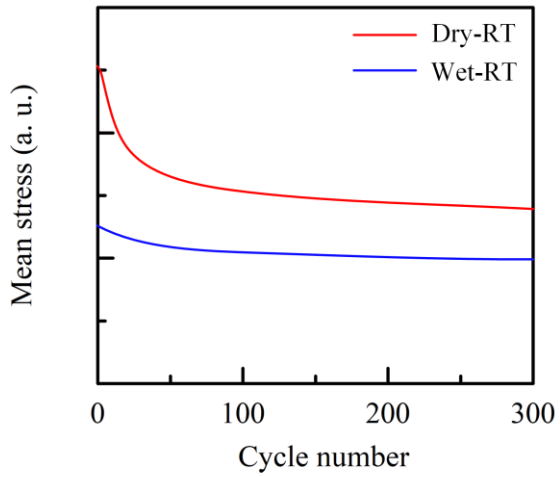


Fig. 7. Mean stress evolution of CF/epoxy interface system under transverse cyclic loads controlled by strain rate at 10^{-6} fs^{-1} as a function of cycle number in dry and wet environments at RT, which shows rapid decrease in initial several cycles, and transits to slower decrease at larger cycles.

3.2 Adhesion properties

After characterizing interfacial mechanical properties, adhesion properties are further measured. Several approaches have been adopted for characterizing interfacial adhesion properties, such as interaction energy between fiber and matrix E_{IE} calculated from equilibration process, fracture energy E_{frac} measured from interfacial peeling or shearing simulation under constant velocity loads, adhesion energy E_{adhe} obtained from interfacial peeling simulation at different pulling rates, and energy barrier E_B determined from interfacial peeling or shearing creep simulation under constant force loads.

Interaction energy E_{IE} between fiber and matrix is measured during final equilibration of interface system, which is calculated using Eq. (1),

$$E_{IE} = \frac{E_f + E_m - E_{f\text{-}m}}{A} \quad (1)$$

where E_f, E_m, and $E_{f\text{-}m}$ represent potential energy of fiber, matrix, and interface system respectively, and A represents interfacial contact area. It is noted that E_{IE} is in a negative value due to attractive interactions between fiber and matrix, and the absolute value is discussed as follows. For GF/epoxy interface, E_{IE} is measured to be 207.9 mJ·m^{-2} as shown in **Table 2**, which is in a good agreement with 174-292 mJ·m^{-2} obtained from contact angle measurement [21, 105]. With SCA incorporation, E_{IE} is increased by 21% to 252.4 mJ·m^{-2}, as SCA poses stronger interactions with matrix than silica [21]. In another study of GF/epoxy interface, E_{IE} is measured as 973 mJ·m^{-2} as shown in **Table 2**, which is in accord with molecular simulations result of silica/epoxy interface (980 mJ·m^{-2}) [26]. It is noted that E_{IE} obtained from different molecular simulations varies, which could be related to different modeling and simulation setups, including boundary conditions of interface model and forcefields in characterizing molecular interactions. For CF/epoxy interface, E_{IE} is 151-174 mJ·m^{-2} as shown in **Table 3**, which is close to experimental and simulation range of 50-250 mJ·m^{-2} [22, 106]. In another study of CF/epoxy, E_{IE} is measured as 1300.2 mJ·m^{-2} [69]. The difference in E_{IE} from different studies of CF/epoxy interface could be resulted from variation of forcefield and simulation setup.

Apart from measurements from equilibration process, adhesion properties are characterized through interfacial deformation. During peeling or shearing simulation under constant velocity loads, the required energy for transferring from intact State *O* to detached State *D* as shown in **Fig. 3** is denoted as fracture energy E_{frac}, which is calculated using Eq. (2),

$$E_{frac} = \frac{E_{intact} - E_{detached}}{A} \quad (2)$$

where E_{intact} and $E_{detached}$ represent potential energy of interface at intact and detached state respectively. From peeling simulation, E_{frac} of GF/PP interface is measured as 11815 mJ·m^{-2},

as shown in **Table 2** [63]. The value is much larger than available experimental measurements of around 1000 mJ·m^{-2}, which could be resulted from significantly larger pulling rates in simulation. Meanwhile, E_{frac} of CF/epoxy interface is measured as 713 mJ·m^{-2} [55], as shown in **Table 3**. From shearing simulation, E_{frac} of CF/epoxy interface is measured as 612 mJ·m^{-2}, which is close to fracture energy of graphite/polymer interface ranging up to 600 mJ·m^{-2} from shearing simulations [107]. E_{frac} increases by 43% after adding functional groups on CF surface, which demonstrates improved interfacial adhesion [102]. It is observed that E_{frac} obtained from shearing simulation is smaller than that from peeling, which indicates weaker resistance of interface to shearing loads, and it corresponds with smaller shear strength compared with tensile strength observed from experiments [13].

By varying pulling rates during interfacial deformation, adhesion energy could be further characterized by measuring mechanical responses during simulations. Peak load f in State A during peeling simulations as shown in **Fig. 3(a)** is related to pulling rate v according to Eq. (3) based on Bell's analysis [108],

$$f = \left(\frac{k_B T}{x_b} \right) \ln v - \frac{k_B T \ln v_0}{x_b} \tag{3}$$

where k_B is Boltzmann constant, T is temperature, x_b is distance parameter, and v_0 is natural bond breaking velocity defined in Eq. (4),

$$v_0 = e^{\left(-\frac{E_{adhe}}{k_B T} \right)} x_b \omega \tag{4}$$

where E_{adhe} is adhesion energy and ω is natural vibration frequency with the value of 1×10^{13} s^{-1}. By varying pulling rates from 2.5 to 40 m·s^{-1} under slow deformation regime, E_{adhe} is quantified using linear regression analysis, which is around 3.2 mJ·m^{-2} for CF/epoxy interface, as shown in **Table 3** [64]. The value is much smaller than interaction energy E_{IE} and fracture energy E_{frac} obtained from previous methods, which could be related to the difference in

simulation and calculation approaches.

For characterizing interfacial adhesion, another approach is by measuring energy barrier under constant force loads. The interface is subjected to peeling and shearing creep as shown in **Fig. 5** and **6** respectively, and energy barrier E_B for breaking non-bonded interactions between fiber and matrix for initiation of creep fracture is obtained. Specifically, creep velocity v_c is related to applied constant load F following Eq. (5) based on Bell's analysis [108],

$$v_c = e^{\left(-\frac{E_B - F x_b}{k_B T}\right)} x_b \omega \tag{5}$$

where v_c is average velocity during creep simulation, which is obtained from dividing maximum creep displacement by simulation time. Based on Bell's analysis, v_c and corresponding F measured at different load levels under low load regime is fitted using Eq. (5), and E_B of peeling and shearing creep is determined. For CF/epoxy interface, E_B of peeling and shearing creep is 4.9 and 4.0 $mJ \cdot m^{-2}$ respectively, as shown in **Table 3** [56, 57, 103]. It is observed that E_B is larger in peeling case, which proves stronger interfacial creep resistance along peeling direction due to larger energy dissipation through matrix elongation.

4. Interfacial degradation under wet environment and loading conditions

Wet or moisture environment is the most typical environmental factor. During the exposure to wet environment, the water is absorbed and diffused into the matrix and interfacial region of FRP composites, which leads to significant degradation of FRP materials, including interfacial mechanical response and adhesion properties, as investigated in previous molecular simulation studies.

4.1 Mechanical properties under wet environment and loading conditions

When interface is conditioned in wet environment, it is subjected to external loads for

measuring variations of mechanical behaviors and properties of interface. Stress-strain curve of interface obtained from peeling simulation under constant velocity loads is shown in **Fig. 3(a)** [64]. In wet environment, the interface shows an elastic regime close to dry case, but reaches peak in State *E* at a smaller strain. Meanwhile, peak stress denoted as tensile strength reduces compared with dry case. It is consistent with experimental observation that strength shows significant degradation, while modulus is less affected by wet environment [13]. In a recent study where five and ten water molecules are added in GF/epoxy interface representing normal and high moisture content cases, tensile strength obtained from peeling simulation decreases by 22% and 31% compared with dry case, as listed in **Table 2** [24]. In another study of GF/VE interface under water immersion, it is found that tensile strength decreases by 26% [75]. In three studies on CF/epoxy interface added with 4, 30 wt% moisture content, and under water immersion, tensile strength decreases by 26%, 59%, and 40% respectively, as listed in **Table 3** [55, 69, 96]. It is observed that the degradation of the interface with a moisture content of 30 wt% is greater than that under water immersion, which could be because that saturated moisture content in interfacial region under water immersion is less than 30 wt% [109]. Moreover, degradation rates are all within experimental measurements range up to 60% [64, 110]. After the peak, the stress shows a sudden linear drop and reaches State *F*, as shown in **Fig. 3(a)**, where matrix fails to resist applied load and debonding occurs in a rapid manner, as shown in **Fig. 3(c)** [64, 72]. As loading continues, the stress shows a continuous decrease as debonding of matrix from fiber progresses continuously, as shown in State *G*. Finally, complete interfacial debonding occurs at a much smaller strain, as shown in State *H*, and elongation of matrix at detached state is smaller [45].

For interface under constant velocity shearing simulation in wet environment, stress-strain curve is shown in **Fig. 4(a)**. The interface reaches stress plateau at a smaller strain compared with dry case, and the plateau level is lower, as matrix is slightly detached from fiber surface

during steady sliding stage in wet case as shown in **Fig. 4(c)**, which is possibly resulted from increased interfacial voids and reduced contact area as discussed previously [55]. Accordingly, IFSS of GF/VE interface shows a reduction of 32% under water immersion [75]. For CF/epoxy interface, IFSS reduces by 38% with 0.5 wt% moisture content, as shown in **Table 3** [72]. Meanwhile, for CF/epoxy interface under water immersion, IFSS is found to reduce by 30% [55]. The decrement of IFSS is close to that of 33% after water immersion for 30 days observed from micro-bond pull-out experiment [55, 111].

Coupled effect of wet environment and sustained loads on mechanical behavior of CF/epoxy interface has been investigated in a recent study [96]. The interface contains 4 wt% moisture content and is subjected to different levels of sustained peeling loads simultaneously, where 25%, 50%, and 75% of interfacial tensile strength are applied as low, medium, and high load level. At low and medium load level, structural changes during peeling creep simulation are similar between dry and wet case. Accordingly, strain increment during 2 ns simulation at low and medium load level is 0.013 and 0.037 respectively, which shows a slight increase compared with values of 0.012 and 0.031 in dry case. During peeling creep simulation at high load level, structural voids tend to initiate around water clusters in matrix during first stage, and then large voids appear around water clusters during second stage. Afterwards, voids grow and expand rapidly, which leads to rapid separation of polymer chains in void region during third stage until interfacial failure. It is indicated that diffused water facilitates initiation of structural voids and accelerates interfacial debonding under sustained loads [96]. With increased mobility of polymer chains affected by water molecules, creep deformation of interface becomes larger within a shorter time compared with dry case. Accordingly, strain increases rapidly and interfacial debonding occurs at 0.20 ns in wet environment, while the interface remains intact in dry environment, which shows weakened resistance to sustained loads [96].

Further molecular investigations focus on interfacial mechanical properties under coupled effect of moisture and cyclic loads. The interface is exposed to transverse cyclic loads with different moisture contents. According to fatigue simulations in wet environment, *S*-*N* curve of CF/epoxy interface is shown in **Fig. 7** [69]. For CF/epoxy interface under coupled effect of 30 wt% moisture content and cyclic loads, initial mean stress *S* decreases significantly by 60%, and by 61% after 300 loading cycles *N*, compared with initial stress level in dry environment, which is larger than the 34% reduction after same cycle number s in dry environment [69]. In wet environment, a large reduction of mean stress level is observed before cyclic loading, which indicates that interfacial properties are already degraded significantly after moisture conditioning, and the effect of subsequent cyclic loads is negligible under moisture effect [69].

From reviewed molecular simulations, degradations of mechanical behaviors and properties under constant velocity tensile, shearing, sustained, and cyclic loads in wet environment have been evidenced, and degradation rate varies from 22%-61%, which is close to the degradation of up to 60% observed in experiments [55, 69, 72, 96, 111].

4.2 Adhesion properties under wet environment and loading conditions

In order to investigate degradations of interfacial bonding quality in wet environment, adhesion properties are examined using various approaches. During equilibration in wet environment, interaction energy E_{IE} between fiber and matrix is calculated based on potential energy of fiber, matrix, and interface using Eq. (1). The variation of absolute value of E_{IE} is discussed as follows. For GF/epoxy interface, E_{IE} variations in wet environment are reported in different studies, as summarized in **Table 2** [21, 24, 26, 69]. Compared with dry cases, E_{IE} of GF/epoxy interface decreases by 22% and 37% with five and ten water molecules respectively [24]. Meanwhile, E_{IE} of GF/epoxy interface with 1 wt% moisture content reduces by 29%. In saturated case where GF/epoxy interface is under water immersion, E_{IE} decreases

by 69% [26]. For CF/epoxy interface, when it is exposed to 30 wt% moisture content condition, E_{IE} even shows a reduction of 96%, as shown in **Table 3** [69]. Moreover, the effect of surface treatment on degradation of E_{IE} in wet environment has been investigated. With SCA coating on GF surface, E_{IE} between SCA-coated silica and epoxy shows a decrement by 24% with 1% moisture content, which is smaller than the 29% reduction without SCA coating, as listed in **Table 2** [21], which indicates improved interfacial resistance to wet environment with SCA coating.

Apart from measurement from equilibration process, interfacial adhesion in wet environment is measured under different loading conditions. Based on constant velocity peeling simulation, enclosed area under stress-strain curve reflects fracture energy E_{frac}. For CF/epoxy interface under water immersion, E_{frac} decreases significantly by 62% as shown in **Table 3** [55]. Based on Eq. (2), E_{frac} of CF/epoxy interface under water immersion shows a reduction of 63% [74]. Meanwhile, the strain at interfacial detachment is much smaller as shown in **Fig. 3(a)**, which indicates significantly reduced interfacial adhesion.

Apart from peeling simulation at a fixed pulling velocity, adhesion energy E_{adhe} is measured at different pulling rates. According to linear regression analysis using Eq. (3) and (4), E_{adhe} of CF/epoxy interface exhibits a reduction of 70% under water immersion, as shown in **Table 3** [64]. The reduction is close to the 69% decrement of E_{IE} of GF/epoxy interface as discussed previously, which indicates similar detrimental effect of water on interfacial adhesion of GF- and CF-bonded interfaces.

From interfacial adhesion results, there is a more severe degradation with increasing moisture content, with degradation rate from 22% to 96% [21, 24, 26, 55, 64, 69, 74]. Meanwhile, for interface under saturated condition, values measured from different methods are quite close, with the range of 62% to 70%, which indicates the effectiveness of these approaches for characterizing interfacial adhesion.

4.3 Degradation mechanism under wet environment and loading conditions

When interface is exposed to wet environment, water molecules form interactions with hydrophilic functional groups of exposed matrix surface, which leads to water absorption on surface, as shown in **Fig. 8(a)** [71]. The increased mobility of matrix at free surface region offers a conduit for absorbed water molecules to diffuse through surface and hoop into entry pores and channels formed due to reduced degree of curing in interior matrix [71]. Successive hopping of water molecules inside surface region of matrix forms a saturated matrix/water interface, which acts as a staging reservoir and leads to subsequent water diffusion into interior structure of matrix and local interface [71]. It is also observed that when diffused water molecules are saturated, they tend to form water clusters due to hydrogen bond (H-bond) interactions with each other [96].

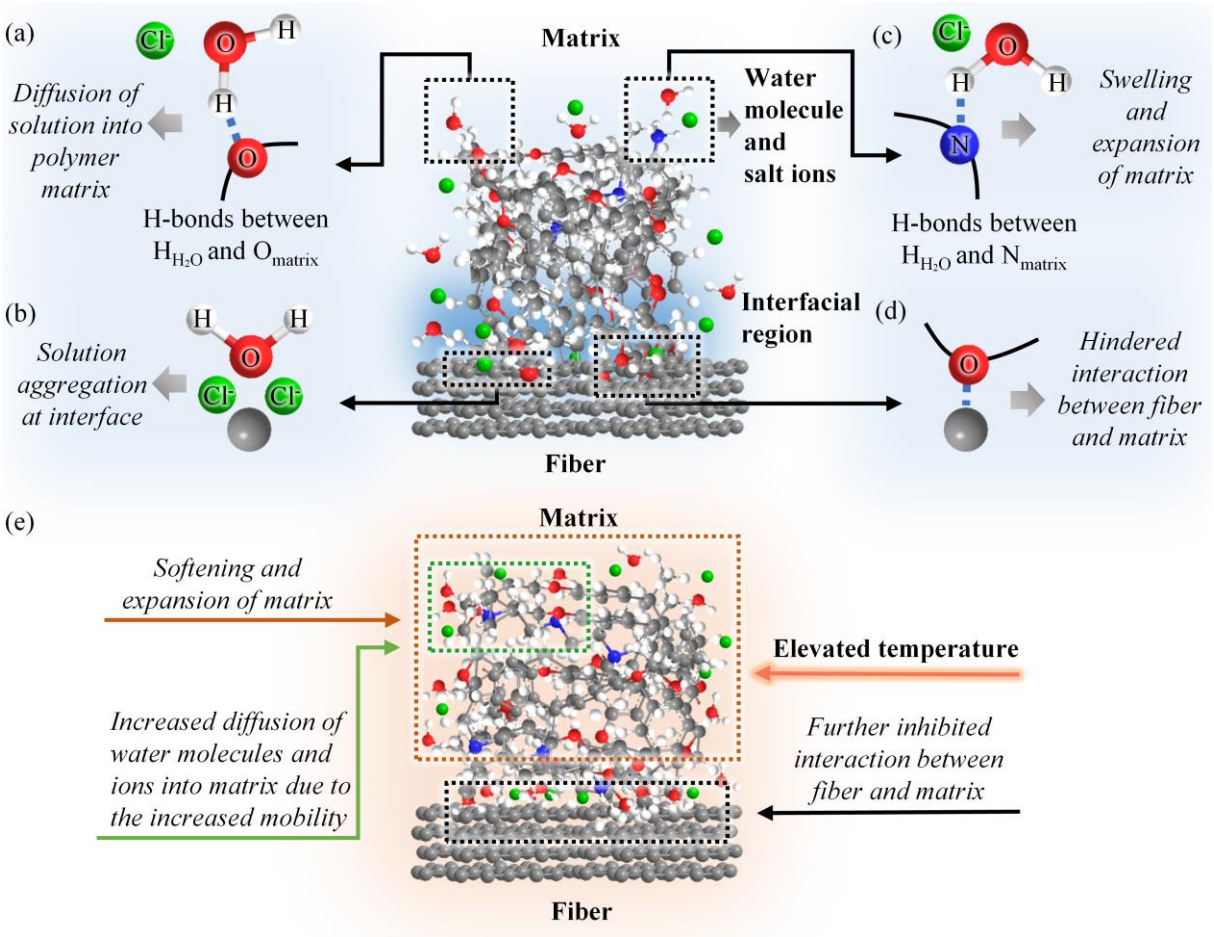


Fig. 8. Degradation mechanisms of fiber/matrix interface in (a-d) wet and salt environments and (e) at elevated temperature. (a) Water molecules and salt ions are absorbed and diffused into matrix due to hydrogen bonds (H-bonds) between water molecules and polymer surface; (b) absorbed water molecules form H-bonds with functional groups on fiber surface, which leads to the aggregation of water molecules at the interface; (c) absorbed water molecules form H-bonds with the matrix structure, which results in the swelling and expansion of matrix; (d) as water molecules form strong interactions with both fiber and matrix, the interaction between fiber and matrix is hindered. Salt ions could further affect the interactions between water molecules and fiber/matrix interface. (e) At elevated temperature, the polymer matrix becomes softened and it allows for increasing diffusion of solution into the matrix, which inhibits the interfacial interaction.

After water diffusion into local interface, absorbed water molecules form interactions with fiber surface. In GF case, silica possesses a hydrophilic surface with hydroxyl groups that interacts closely with water molecules. Accordingly, radial distribution function (RDF) between hydroxyl groups on silica surface (H_{Si} and O_{Si}) and water molecules (O_{H_2O} and H_{H_2O}) is measured to characterize the distribution between water and silica surface, where RDF represents the probability of finding an O_{H_2O} or H_{H_2O} atom at a distance from referenced H_{Si} or O_{Si} atom, as shown in **Fig. 9(a)**. It is found that RDF of H_{Si}-O_{H_2O} and O_{Si}-H_{H_2O} exhibits noticeable peaks at 0.21 and 0.29 nm respectively, which indicates that water molecules are aggregated around silica surface [45]. In order to characterize interactions between water and silica, H-bond number between water and silica is quantified, which is considered to form when distance between donor and acceptor atom of hydrogen is less than 0.33 nm and donor-hydrogen-acceptor angle is within 110°-180° [45]. As distance and angle between atoms of water and silica surface meet the criteria for H-bond formation, it is considered that some absorbed water molecules could form H-bonds with silica and seize the functional sites on silica surface originally occupied by matrix, as shown in **Fig. 8(b)**. It demonstrates that local

aggregation of water molecules affects interactions between fiber and matrix and leads to interfacial expansion with increased interfacial width [26, 45, 112].

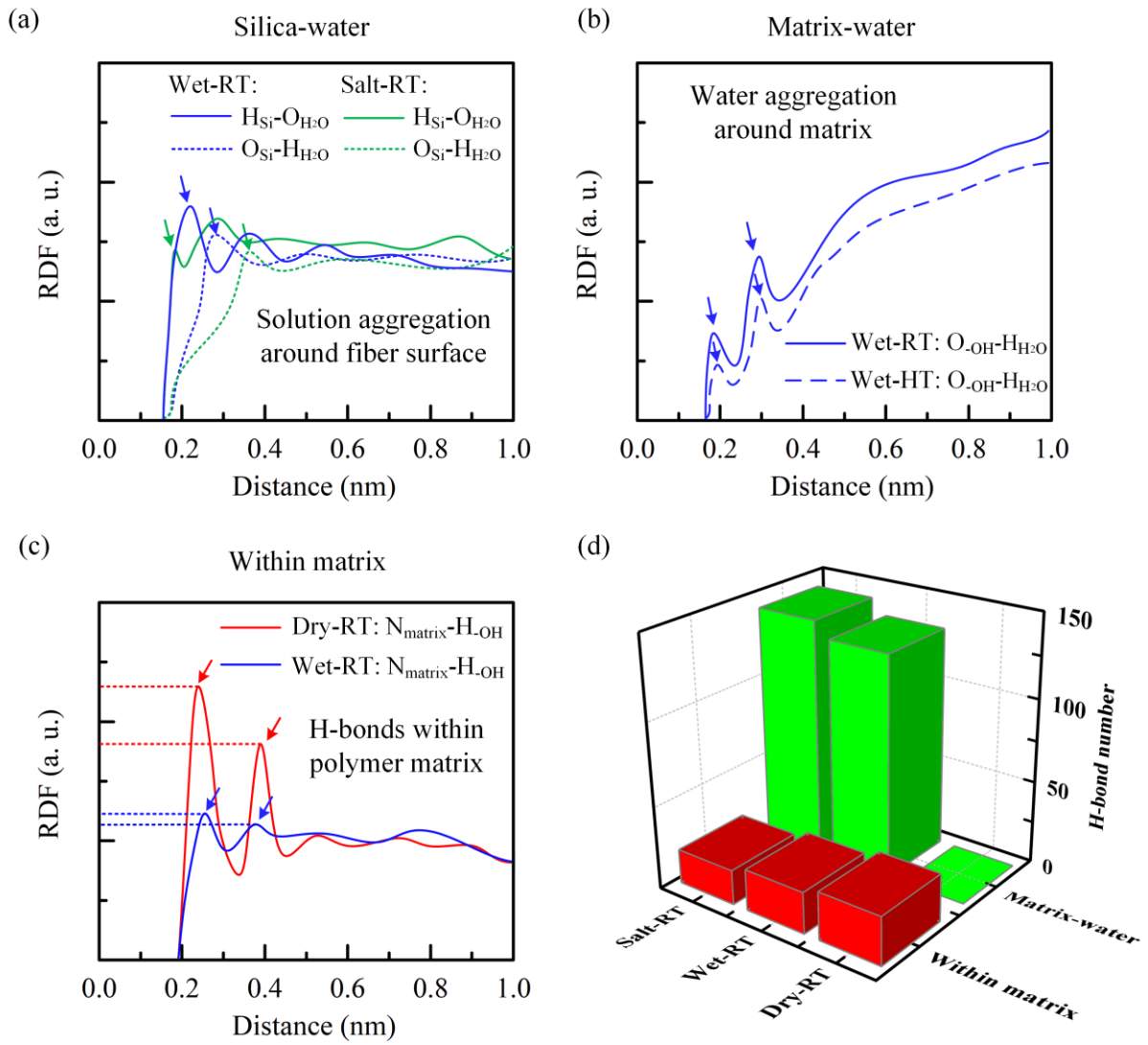


Fig. 9. Radial distribution function (RDF): (a) between hydroxyl groups (H_{Si}, O_{Si}) on silica surface and water molecules (O_{H_2O}, H_{H_2O}) in wet and salt environments at RT; (b) between hydroxyl groups (O_{-OH}) of matrix and hydrogen atoms of water (H_{H_2O}) at RT and high temperature (HT); and (c) between nitrogen atoms (N_{matrix}) and hydroxyl groups (H_{-OH}) within matrix in dry and wet environments at RT. (d) Number of H-bonds formed between matrix and water, and within matrix in dry, wet, and salt environments at RT.

For diffused water molecules to local interfacial region, interactions with matrix are of highly concern. In study on CF/epoxy interface, RDF between hydrophilic functional groups of matrix and hydrogen atoms of water molecules (H_{H_2O}) possesses two noticeable peaks at around 0.20 and 0.30 nm, as shown in **Fig. 9(b)**. The peaks infer local aggregation of water molecules around functional groups in matrix, as shown in **Fig. 8(c)**. Similar peak positions are observed between nitrogen atoms in matrix (N_{matrix}) and H_{H_2O} in GF/epoxy interface [45]. By examining H-bond formation, it is found that H-bond number formed between functional groups of matrix with the size of $5.9 \times 5.9 \times 4.7$ nm^3 and O_{H_2O} is 133 ± 6, as shown in **Fig. 9(d)**, which indicates strong interactions between water and matrix [47]. Accordingly, water molecules affect inter- and intramolecular interactions within matrix, which is characterized by RDF between N_{matrix} and hydrogen atoms in hydroxyl groups (H_{-OH}) of matrix, as shown in **Fig. 9(c)**. There are two noticeable peaks at 0.22 and 0.40 nm, which indicates existence of inter- and intramolecular H-bonds within matrix. Notably, peak values decrease obviously in wet environment, which infers that inter- and intramolecular interactions within matrix reduce significantly by absorbed water molecules. Accordingly, H-bond number formed between functional groups within matrix is found to reduce from 26 ± 3 to 22 ± 3, as shown in **Fig. 9(d)** [47]. Meanwhile, non-bonded interaction energy within matrix reduces by 19% [55]. Inhibited interactions within matrix lead to reduced potential energy and higher mobility of matrix, which results in swelling and expansion of matrix at local interface, and lead to mismatches between fiber and matrix as fiber possesses stronger dimensional stability. Consequently, it increases interfacial voids and therefore diffusion of water molecules to local interface is accelerated.

As a result of strong interactions of aggregated water molecules with fiber and matrix, interfacial interactions are altered, as shown in **Fig. 8(d)**. Electrostatic interaction energy decreases by 73% in wet environment, which infers that interfacial interactions could be inhibited by water molecules, and results in degraded mechanical behaviors of interface as

discussed in section 4.1 [45]. For CF/epoxy interface under constant velocity peeling loads, hair-like bridge is formed as residual polymer molecules are attached to fiber surface during debonding, which impedes interfacial detachment in dry environment, as shown in **Fig. 3(b)**. Comparatively, hair-like bridge is not distinct due to reduced interfacial interactions in wet environment, which cannot impede interfacial debonding, as shown in **Fig. 3(c)** [55]. Therefore, interfacial interactions are weakened by absorbed water molecules, which reduces interfacial bonding and close contact, and leads to degraded mechanical and adhesion properties as discussed in section 4.1 and 4.2, degrading interfacial integrity consequently [45].

5. Interfacial degradation under salt environment and loading conditions

For FRP structure in offshore or marine engineering, it is continuously exposed to salt environment, which is more complex compared with wet environment. Currently, several molecular investigations have been conducted focusing on the degradation of fiber/matrix interface in salt environment, including variations of interfacial mechanical response and adhesion properties.

5.1 Mechanical properties under salt environment and loading conditions

After conditioned in salt environment, the interface is subjected to external loads for characterizing degradations of mechanical behaviors and properties. According to peeling stress-strain curve, stress evolution under elastic regime of interface immersed in saltwater is similar as dry and wet cases, but it reaches peak stress at a much smaller strain, as interface shows an obvious detachment after pulling for a small distance [47, 64, 75]. Tensile strength of GF/VE interface under saltwater immersion decreases by 29%, which shows a larger decrement compared with wet case (26%) [75]. In recent two studies of CF/epoxy interface, tensile strength decreases by 27% and 47%, as listed in **Table 3**, which is larger than the

reduction of 26% and 40% in wet case [47, 96]. After the peak, the stress shows a sudden and rapid decrease to zero, and debonding is similar as wet case, which indicates that the effect of salt ions on peeling deformation is not obvious.

Apart from constant velocity peeling simulation, mechanical degradation of GF/VE interface under constant velocity shearing loads is investigated [75]. From shearing stress-strain curves, the plateau stress level further reduces compared with wet case, as interface shows a large debonding area during shearing [75]. Accordingly, IFSS of GF/VE interface shows a decrement of 39%, which is larger than wet case (32%) [75]. It indicates further degradation of interfacial shear properties caused by salt ions.

Under coupled effect of salt environment and sustained loads, mechanical behavior of CF/epoxy interface is further investigated [96]. At low load levels, increment of creep strain during 2 ns simulation is 0.011 in salt environment, which shows a slight reduction compared with wet case (0.013) and dry case (0.012). Meanwhile, at medium load level, creep strain increment is 0.035 in salt case, which reduces compared with wet case (0.037), while it is larger than dry case (0.031). Furthermore, at high load level, detachment time is 0.22 ns, which is slightly longer than 0.20 ns in wet case, while no detachment occurs in dry case. Simulation results demonstrate that addition of salt ions could lead to slight reduction on creep strain and elongation of detachment time compared with wet case, which indicates that the detrimental effect is not that obvious in salt environment. Meanwhile, creep evolution is still accelerated compared with dry case, which indicates that creep resistance of interface is still weakened.

From these studies on mechanical degradation of interface in salt environment, tensile strength shows a reduction of 1%-7% compared with wet case due to addition of salt ions, which is close to reduction of 3%-10% observed in experiments [45, 47, 64, 75, 96, 113]. Comparatively, for creep behavior, the degradation is not that obvious compared with wet case, while creep resistance is still weakened compared with dry case. The reason for the difference

of interfacial behaviors under constant velocity and under sustained loads as affected by salt ions is not elucidated. Meanwhile, it is still not clear about mechanical behaviors under cyclic loads in salt environment, which require further investigation.

5.2 Adhesion properties under salt environment and loading conditions

To better understand effect of salt ions, degradations of interfacial adhesion are further evaluated. According to structural equilibration of GF/epoxy interface in salt environment, interaction energy E_{IE} between silica and epoxy is calculated using Eq. (1), which decreases by 75% under saltwater immersion compared with dry case, as shown in **Table 2**, exhibiting a larger reduction compared with wet case (69%) [45]. The larger reduction indicates that salt environment possesses a more detrimental effect on interfacial adhesion.

After equilibration process, interfacial deformation is carried out to measure interfacial adhesion in salt environment. Based on peeling simulation at various pulling rates, interfacial adhesion is characterized. From linear regression analysis using Eq. (3) and (4), adhesion energy E_{adhe} of CF/epoxy interface exhibits a significant drop of 75% compared with dry case, which is larger than the 70% decrement in wet case, as summarized in **Table 3**, indicating that salt ions results in further degradation of interfacial adhesion [64].

By comparing degradations of interfacial adhesion measured from different methods, interfacial adhesion in salt environment shows a decrement of around 75% for both GF/epoxy and CF/epoxy interfaces, and the larger reduction than wet case indicates further interfacial degradation caused by salt ions [45, 64].

5.3 Degradation mechanism under salt environment and loading conditions

When interface is conditioned in salt environment, absorption of water molecules together with salt ions into matrix and interface further affects interactions of fiber and matrix, and

between bonded materials. Particularly, salt ions further affect interactions between water molecules and fiber surface. From RDF of H_{Si}-O_{H_2O} and O_{Si}-H_{H_2O} in GF/epoxy interface, the distance of first noticeable peaks changes from 0.21 and 0.29 nm in wet case to 0.18 and 0.37 nm respectively, as shown in **Fig. 9(a)**. Meanwhile, values of both peaks reduce, which infers that localization of water molecules around silica surface and H-bond formation between silica and water are inhibited compared with wet case, and it leads to slight increase of interfacial porosities.

Salt ions absorbed into interface could affect interactions between water molecules and matrix as discussed previously. For CF/epoxy interface, RDF between functional groups of matrix and H_{H_2O} shows similar shapes and peak positions as wet case [64]. Meanwhile, H-bond number between functional groups of matrix and O_{H_2O} increases to 142 ± 9 compared with 133 ± 6 in wet case, as shown in **Fig. 9(d)** [47]. The larger value of H-bond number indicates that salt ions facilitate H-bond formation between matrix and water molecules. For inter- and intramolecular interactions within matrix, H-bond number within matrix reduces slightly from 22 ± 3 in wet case to 21 ± 2 in salt case, as shown in **Fig. 9(d)**, which indicates salt ions further inhibit H-bond formation within matrix [47]. Similar results have been observed in GF/VE interface, where peak value of RDF between functional groups within matrix reduces significantly by 65% in salt environment compared with dry case [75]. However, for GF/epoxy interface, it is reported that the two local peaks of N_{matrix}-H_{H_2O} RDF in wet environment as shown in **Fig. 9(b)** become less obvious in salt environment, which indicates that local aggregation of water molecules around matrix and H-bond formation between matrix and water could be inhibited by salt ions [45]. The discrepancy between results from CF- and GF-bonded interface could be related to different measurements of RDF, where in CF-bonded interface, RDF is between functional groups of matrix and water, while in GF-bonded interface, RDF is between nitrogen atoms of matrix and water. Nevertheless, there are

consistent reduced interactions within matrix in salt environment, which causes increased mobility of matrix and swelling of matrix at interface, which further decreases local contact at interface, and consequently results in more saltwater ingress into interface [47].

With addition of salt ions, interactions between water molecules and interface become stronger compared with wet case, which further inhibit interactions and H-bond formation between fiber and matrix, as shown in **Fig. 8(d)**. Accordingly, from RDF between H_{Si} and O_{OH} of VE matrix, first peak value reduces significantly by 81% compared with dry case [75]. As a result, interfacial bonding condition and contact further reduce, and it leads to more severe degradation of mechanical and adhesion properties as discussed in section 5.1 and 5.2, which consequently result in degraded interfacial integrity [45]. Comparatively, for GF/epoxy interface, interactions between water molecules and interface could be inhibited by salt ions, which leads to less diffusion of water molecules at interface, and decreased interfacial porosities [45]. Given different molecular interactions observed from CF- and GF-bonded interface, it is expected that future researches could be conducted to compare molecular behaviors of different interfaces systematically and further explore underlying mechanisms of the effect of salt ions on different interfaces.

6. Interfacial degradation under elevated temperature and loading conditions

Apart from water or water-based solutions, elevated temperature due to sunlight has been found to possess a driving effect on the ageing process of composite structure, which affects the matrix and the resulted fiber/matrix interface. Recently, great efforts have been contributed to characterizing the properties of fiber/matrix interface under different levels of temperature.

6.1 Mechanical properties under elevated temperature and loading conditions

When interface is conditioned at elevated temperature, degradation of mechanical responses is characterized. From peeling stress-strain curve under constant velocity simulation, the stress increase under elastic regime is similar as room temperature (RT) cases, while peak stress reduces monotonously with increasing temperature [47, 55]. In a recent study of GF/PP interface, tensile strength shows 13% loss at 130 °C compared with that at 25 °C, as shown in **Table 2** [63]. Compared with 27 °C cases, tensile strength of GF/VE interface shows degradation of 21%, 9% and 28% in 67 °C dry, wet, and salt environment respectively [75]. Maximum degradation rate compared with 27 °C dry case is 47% in 67 °C salt case. For CF/epoxy interface, tensile strength reduces by around 13% in 50 °C dry, water, and saltwater immersed cases compared with 27 °C cases respectively, as listed in **Table 3** [47]. Largest reduction is 55% in 50 °C saltwater environment compared with 27 °C dry case. In a recent study on CF/epoxy interface, tensile strength shows a decrement of around 16% when temperature increases from 25 to 81 °C in wet and salt cases, and reaches a maximum of 39% degradation in 81 °C salt environment compared with 25 °C dry case, as listed in **Table 3** [96]. The obvious degradation of mechanical properties at elevated temperature is resulted from softened matrix structure and decreased number of molecules bonded to fiber surface during debonding [55].

Mechanical degradation of interface at HT is also determined using constant velocity shearing simulation [55]. For GF/VE interface, IFSS at 67 °C decreases by around 19% in dry, wet, and salt environments compared with 27 °C cases [75]. Compared with 27 °C dry case, IFSS of CF/epoxy interface exhibits 30% and 38% reduction in 50 °C dry and wet case respectively, as shown in **Table 3** [55]. Degradation rate of 30%-38% in hygrothermal environment agrees with the 41% reduction of IFSS measured from micro-bond experiment, which demonstrates the detrimental effect of hygrothermal environment on interfacial

mechanical properties [55, 114]. The larger reduction of CF/epoxy interface from shearing simulation compared with that of 13%-16% from peeling simulations indicates that at HT, CF/epoxy interface could exhibit a larger degradation in terms of shearing properties compared with tensile properties [13].

When interface is subjected to sustained loads in hygrothermal environment, creep performance of CF/epoxy interface is explored [96]. It is found that in wet and salt environments, creep behaviors are highly temperature-dependent. At low load level, the interface exhibits a larger creep strain with increasing temperature. Comparatively, at medium load level, the interface transits from intact to detached state at HT. Moreover, at high load level, the interface shows a faster debonding at HT [96]. It indicates that creep strain evolution is accelerated at elevated temperature, especially in hygrothermal environment.

For the HT effect, variations of debonding behavior and interfacial strength have been obtained. With increasing temperature, degradation rate varies within 13%-30% in dry environment, which is within 13%-28% in hygrothermal environment [47, 55, 63, 75, 96]. Meanwhile, compared with RT dry case, largest reduction could reach 38%-55% in hygrothermal environment [47, 55, 75]. Nevertheless, investigation on mechanical degradation under cyclic loads at HT is still lacking.

6.2 Adhesion properties under elevated temperature and loading conditions

Interfacial adhesion properties at elevated temperature are characterized both during equilibration and under loads. For GF/epoxy interface conditioned in 87 °C dry and water immersion environments, interaction energy E_{IE} decreases by 12% and 6% compared with 27 °C cases respectively, as listed in **Table 2** [63]. Compared with 27 °C dry case, largest reduction of 71% is observed in 87 °C water immersion, which agrees well with the degradation up to 71% as observed from glass fiber-reinforced polymer (GFRP) composite plates in

hygrothermal environment [115]. It is observed that hygrothermal environment shows most detrimental impact on interfacial adhesion properties.

After reaching fully equilibrated state, adhesion properties are further examined under loads. From constant velocity peeling simulation, E_{frac} of GF/PP interface decreases by 24% with temperature increasing from 25 to 130 °C, as shown in **Table 2**, which is consistent with degradation trend of interfacial fracture energy in experiments of GFRP composite [63, 116]. For CF/epoxy interface, compared with 27 °C dry and wet cases, E_{frac} reduces by 11% and 17% in 50 °C dry and water immersion environment respectively, as shown in **Table 3** [55]. Largest reduction is up to 69% in 50 °C water immersion, which demonstrates severe degradation of interfacial adhesion in hygrothermal environment.

Through peeling simulations at different pulling rates, adhesion energy E_{adhe} of interface is obtained to further characterize interfacial degradation at HT. By conducting linear regression analysis using Eq. (3) and (4), E_{adhe} is obtained accordingly. Compared with 27 °C dry, water, and saltwater conditions, E_{adhe} of CF/epoxy interface shows a reduction of around 13% in 50 °C cases respectively, as shown in **Table 3**. Largest reduction of 78% appears in 50 °C salt environment compared with 27 °C dry case, which agrees with largest degradation of properties ranging from 46% to 81% for carbon fiber-reinforced polymer composite in hygrothermal environment [47].

For interfacial adhesion properties at elevated temperature, degradation rate ranges from 11% to 24% at HT in dry environment, and is 6%-17% in hygrothermal environment, which is close to experimental measurement of around 17% reduction for shear strength [13, 47, 55, 63]. Meanwhile, in hygrothermal environment, interfacial adhesion properties exhibit most severe reduction from 69% to 78% compared with RT dry case, which demonstrates that interfacial degradation in hygrothermal environment requires special concern.

6.3 Degradation mechanism under elevated temperature and loading conditions

At elevated temperature, from RDF of N_{matrix}-H_{-OH} within matrix, value of two noticeable peaks as observed in **Fig. 9(c)** shows a monotonous reduction at elevated temperatures, which indicates that inter- and intramolecular interactions within matrix reduce [26]. Similarly, for GF/VE interface, with increasing temperature from 27 to 87 °C, peak value of RDF between oxygen atoms in ester groups ($O_{-C=O}$) and H_{-OH} within matrix shows 32% reduction [75]. Meanwhile, non-bonded interaction energy within matrix decreases from 3772.0 ± 6.9 to 3708.5 ± 8.9 kcal·mol^{-1} when temperature increases from 27 to 50 °C [55]. Weakened inter- and intramolecular interactions within matrix at HT lead to softened matrix structure, and schematic diagram is shown in **Fig. 8(e)**.

In hygrothermal environment, absorption and diffusion of water and saltwater are influenced, which consequently affects interfacial structure and properties. Specifically, glass transition temperature of matrix decreases from 185.5 °C in dry environment to 109.3 and 99.5 °C in wet and salt environments, where matrix is close to glass transition state and becomes softened in hygrothermal environment [55, 71]. From RDF of $O_{-C=O}$-H_{-OH} within VE matrix, local peak value decreases by 46% in 87 °C salt environment compared with 27 °C case, which indicates weakened tendency to form H-bonds within matrix at elevated temperature [75]. Moreover, non-bonded interaction energy within matrix in wet environment reduces from 3048.2 ± 9.7 to 2940.7 ± 18.9 kcal·mol^{-1} when temperature increases from 27 to 50 °C [55]. It is expected that softened matrix structure provides more pores and channels for further diffusion of solution into matrix and interface compared with RT cases, as shown in **Fig. 8(e)**, which facilitates severe interfacial swelling. Increased absorption and diffusion of solution affects interactions between water molecules and interface. From RDF curve of N_{matrix}-H_{H_2O} as shown in **Fig. 9(b)**, local peak values decrease at elevated temperature, which indicates that aggregation of water molecules around matrix and H-bond formation between

matrix and water could be inhibited [26]. Comparatively, from RDF between H_{Si} and O_{-OH} of VE matrix, first peak value reduces by 40% and 48% in 87 °C dry and salt environments compared with 27 °C cases respectively, which indicates that tendency for interfacial H-bond formation is inhibited [75]. Furthermore, for interfacial interactions, electrostatic energy shows a decrease of 7% and 25% at 87 °C dry and wet cases compared with 27 °C cases respectively, which infers that interfacial interactions decrease at elevated temperature, as shown in **Fig. 8(e)** [26]. Meanwhile, with softened matrix structure, fewer hair-like bridges at interface are observed during interfacial separation, and thus resistance to interfacial debonding decreases [55]. In hygrothermal environment, accelerated water diffusion decreases fiber/matrix interactions and thus reduces interfacial contact area, which accounts for most severe degradation of mechanical and adhesion properties as discussed in section 6.1 and 6.2, and results in worst interfacial integrity.

7. Summary and future challenges

In this paper, molecular details of degradation of fiber/matrix interfaces under environmental and loading conditions and underlying mechanisms are reviewed, including modeling and simulation approaches of molecular fiber/matrix interfaces, interfacial properties and adhesion, interfacial degradation under different experimental and load exposures and underlying degradation mechanisms. Specifically, the modeling of interfaces involves the construction of glass and carbon fibers, and thermosetting and thermoplastic matrixes. Meanwhile, simulation setups of wet, salt, and elevated temperature environments, and constant velocity, sustained, and cyclic loads together with the used forcefields are introduced. Afterwards, the methods for characterizing the mechanical and adhesion properties of the interfaces are discussed. Moreover, the degradations of interfacial behaviors and properties in wet, salt, elevated temperature environments, and under loading conditions are introduced, and

underlying mechanisms of interfacial degradation under different environmental conditions are discussed.

Previous studies have provided valuable insights into interfacial degradation and underlying mechanisms, while there exists some differences in modeling and simulation compared with experiments, including modeling of fiber surface and matrix, simulation of water diffusion, temperature gradient, chemical interactions, and bond breaking. In order to address these limitations in future investigations, some suggestions on future molecular simulations of interface are proposed. For rough surface and surface treatment of fiber, fiber models in molecular simulation could be designed in woven structure with puncture and coated with sizing agents. Meanwhile, matrix model with voids and impurities could be constructed by manually removing some monomers and inserting some impurities according to experimental observations [117]. Afterwards, large-size interface model could be immersed in solution environments at different temperatures to simulate absorption and water molecules from surrounding environment to interior of matrix and interface, as well as temperature gradients between surface and core of interface model. After different durations of environmental exposure, the interface could be examined under coupled effects of environments together with loading conditions. During simulations, molecular interactions could be characterized using reactive forcefield, and interfacial changes with occurrence of chemical reactions could be captured during environmental conditioning, and bond-breaking behaviors under loads could be recorded. After considering these molecular details of interface, more accurate interfacial modeling and simulation could be achieved, which enables the exploration of interfacial degradation mechanisms under more realistic and complicated conditions, and provides direct relationship with behaviors of composite materials subjected to various environmental and loading conditions in real applications.

Based on these molecular simulation works, the load-displacement curves, mechanical

properties, and adhesion properties of fiber/matrix interface are used to obtain stress-strain relationship of interface under investigated conditions using theoretical analysis, which are used as inputs to develop constitutive models of interface under environmental and loading conditions. Apart from fiber/matrix interface, degraded mechanical properties of fiber and matrix under different environmental and loading conditions obtained from molecular simulation are used to establish the constitutive models of fiber and matrix, respectively. The derived constitutive models of fiber, matrix, and interface under different environment and loading conditions could be applied in continuum model of composite under investigated conditions. With the developed continuum model, the relationship between property degradation of composite and investigated load and environmental conditions could be obtained. By substituting the relationship into Arrhenius accelerating theory and time-temperature equivalent theory, the degradation rate of composite under investigated conditions could be obtained, which could be used to predict the properties of composite during intended service life, so as to develop the prediction model of composite [118-120]. The predicted properties degradations of composite are compared with experiment results of composite exposed to short-term environment and loading conditions to validate the prediction model. Afterwards, the prediction model is further modified by comparing with long-term experiment results to improve the prediction accuracy, so as to obtain a more accurate prediction model on long-term properties of composite under real service conditions. It is expected that with the developed multiscale simulation paradigm and prediction model, it contributes to the fundamental understanding of FRP composite degradation affected by surrounding environment and loads, and enables the prediction of properties degradation of FRP composite during long-term service life, which contributes to refine the design guideline of practical engineering applications and civil constructions of composite.

Acknowledgements

The authors acknowledge supports from National Natural Science foundation of China [grant number 51808020 and 51978025] and China Postdoctoral Science Foundation [grant number 2018T110029].

References

[1] V.M. Karbhari, J.W. Chin, D. Hunston, B. Benmokrane, T. Juska, R. Morgan, J.J. Lesko, U. Sorathia, D. Reynaud, Durability Gap Analysis for Fiber-Reinforced Polymer Composites in Civil Infrastructure, Journal of Composites for Construction 7(3) (2003) 238-247.

[2] J.S. Dolado, K. van Breugel, Recent advances in modeling for cementitious materials, Cement and Concrete Research 41(7) (2011) 711-726.

[3] D. Kendall, The business case for composites in construction, Reinforced Plastics 52(7) (2008) 20-27.

[4] T. Keller, Recent all-composite and hybrid fibre-reinforced polymer bridges and buildings, Progress in Structural Engineering and Materials 3(2) (2001) 132-140.

[5] O. Hag-Elsafi, S. Alampalli, J. Kunin, Application of FRP laminates for strengthening of a reinforced-concrete T-beam bridge structure, Composite Structures 52(3-4) (2001) 453-466.

[6] G. Hota, R. Liang, Advanced fiber reinforced polymer composites for sustainable civil infrastructures, ISISS' 2011;International symposium on innovation & sustainability of structures in civil engineering, 2011.

[7] J. Smits, Fiber-Reinforced Polymer Bridge Design in the Netherlands: Architectural Challenges toward Innovative, Sustainable, and Durable Bridges, Engineering 2(004) (2016) 518-527.

[8] F.A. Hai, B.B. Yu, C. Wl, A. Yq, A. Jw, Connections and structural applications of fibre reinforced polymer composites for civil infrastructure in aggressive environments, Composites Part B: Engineering 164 (2019) 129-143.

[9] T.Q. Liu, J.Q. Yang, P. Feng, K.A. Harries, Determining rotational stiffness of flange-web junction of pultruded GFRP I-sections, Composite Structures 236 (2020) 111843.

[10] V.M. Karbhari, J.W. Chin, D. Hunston, B. Benmokrane, T. Juska, R. Morgan, J.J. Lesko, U. Sorathia, D. Reynaud, Durability Gap Analysis for Fiber-Reinforced Polymer Composites in Civil Infrastructure, Journal of Composites for Construction 7(3) (2003) 238-247.

[11] H.R. Hamilton, B. Benmokrane, C.W. Dolan, M.M. Sprinkel, Polymer Materials to Enhance Performance of Concrete in Civil Infrastructure, Polymer Reviews 49(1) (2009) 1-24.
[12] L.C. Hollaway, A review of the present and future utilisation of FRP composites in the civil infrastructure with reference to their important in-service properties, Construction & Building Materials 24(12) (2010) 2419-2445.
[13] T.Q. Liu, X. Liu, P. Feng, A comprehensive review on mechanical properties of pultruded FRP composites subjected to long-term environmental effects, Composites Part B Engineering 191 (2020) 107958.
[14] A. Rolland, K. Benzarti, M. Quiertant, S. Chataigner, Accelerated Aging Behavior in Alkaline Environments of GFRP Reinforcing Bars and Their Bond with Concrete, Materials 14(19) (2021) 5700.
[15] F. Shalchy, N. Rahbar, Nanostructural Characteristics and Interfacial Properties of Polymer Fibers in Cement Matrix, Acs Applied Materials & Interfaces 7(31) (2015) 17278.
[16] S.-P. Ju, C.-C. Chen, T.-J. Huang, C.-H. Liao, H.-L. Chen, Y.-C. Chuang, Y.-C. Wu, H.-T. Chen, Investigation of the structural and mechanical properties of polypropylene-based carbon fiber nanocomposites by experimental measurement and molecular dynamics simulation, Computational Materials Science 115 (2016) 1-10.
[17] C. Wu, R. Wu, J. Jiang, L.-h. Tam, Recent advances in understanding environmental effects on deterioration of carbon fiber/epoxy matrix interface in civil engineering applications via molecular simulation, Acta Materiae Compositae Sinica 37(12) (2020) 2941-2952.
[18] C. Wu, R. Wu, L.-h. Tam, Understanding Degradation of Fiber/Matrix Interface Under Environmental Effects Using Molecular Simulation, CICE 2021: 10th International Conference on FRP Composites in Civil Engineering, Springer International Publishing, Cham, 2022, pp. 2096-2108.
[19] D. Lau, Q. Qiu, A. Zhou, C.L. Chow, Long term performance and fire safety aspect of FRP composites used in building structures, Construction and Building Materials 126 (2016) 573-585.
[20] P. Wang, Q. Yang, M. Wang, D. Hou, J. Zhang, Theoretical investigation of epoxy detachment from C-S-H interface under aggressive environment, Construction and Building Materials 264 (2020) 120232.
[21] M.T. Stoffels, M.P. Staiger, C.M. Bishop, Reduced interfacial adhesion in glass fibre-epoxy composites due to water absorption via molecular dynamics simulations, Composites Part A: Applied Science and Manufacturing 118 (2019) 99-105.

[22] S. Kasahara, J. Koyanagi, K. Mori, M. Yabe, Evaluation of interface properties of carbon fiber/ resin using the full atomistic model considering the electric charge state, Advanced Composite Materials 30(9) (2020) 164-175.
[23] S.A. Mian, L.C. Saha, J. Jang, L. Wang, X. Gao, S. Nagase, Density Functional Theory Study of Catechol Adhesion on Silica Surfaces, The Journal of Physical Chemistry C 114(48) (2010) 20793-20800.
[24] C. Higuchi, H. Tanaka, K. Yoshizawa, Molecular Understanding of the Adhesive Interactions between Silica Surface and Epoxy Resin: Effects of Interfacial Water, Journal of Computational Chemistry 40 (2019) 164-171.
[25] W. Jian, L.-h. Tam, D. Lau, Atomistic study of interfacial creep behavior in epoxy-silica bilayer system, Composites Part B: Engineering 132 (2018) 229-236.
[26] X.Q. Wang, W. Jian, O. Büyüköztürk, C.K.Y. Leung, D. Lau, Degradation of epoxy/glass interface in hygrothermal environment: An atomistic investigation, Composites Part B Engineering 206 (2020) 108534.
[27] F. Ebrahem, B. Markert, Molecular dynamics simulations of the cooling rate influence on the tensile strength of silica glass, Proceedings in Applied Mathematics and Mechanics 17(1) (2017) 235-236.
[28] V.S. Shiryaev, M.F. Churbanov, G.E. Snopatin, F. Chenard, Preparation of low-loss core–clad As–Se glass fibers, Optical Materials 48 (2015) 222-225.
[29] C. Jiang, X. Wang, M. Zhu, H. Xu, Preparation of chalcogenide glass fiber using an improved extrusion method, Optical Engineering 55(5) (2016) 1-8.
[30] F. Liu, H. Wang, L. Xue, L. Fan, Z. Zhu, Effect of microstructure on the mechanical properties of PAN-based carbon fibers during high-temperature graphitization, Journal of Materials Science 43(12) (2008) 4316-4322.
[31] C. Li, A.R. Browning, S. Christensen, A. Strachan, Atomistic simulations on multilayer graphene reinforced epoxy composites, Composites Part A: Applied Science and Manufacturing 43(8) (2012) 1293-1300.
[32] C.M. Hadden, D.R. KlimekMcDonald, E.J. Pineda, J.A. King, R.A. M., Mechanical properties of graphene nanoplatelet/carbon fiber/epoxy hybrid composites: Multiscale modeling and experiments, Carbon 95 (2015) 100-112.
[33] V. Fiore, A. Valenza, Epoxy resins as a matrix material in advanced fiber-reinforced polymer (FRP) composites, Woodhead Publishing2013.
[34] S.C. Chowdhury, R. Prosser, T.W. Sirk, R.M. Elder, J.W. Gillespie, Glass fiber-epoxy

interactions in the presence of silane: A molecular dynamics study, Applied Surface Science 542 (2021) 148738.
[35] L. Liu, C. Jia, J. He, F. Zhao, D. Fan, L. Xing, M. Wang, W. Fang, Z. Jiang, Y. Huang, Interfacial characterization, control and modification of carbon fiber reinforced polymer composites, Composites Science and Technology 121(1) (2015) 56-72.
[36] K. Lin, T. Yu, Debonding simulation of fibre-matrix interfaces of FRP composites with reactive force field, Construction and Building Materials 312 (2021) 125304.
[37] B. Li, Y. Lv, J. Chen, L. Huang, X. Zhang, Fatigue performance of carbon fiber reinforced epoxy resin: A molecular simulation, Polymers for Advanced Technologies 32(4) (2020) 1518-1530.
[38] G. Gibson, Chapter 27 - Epoxy Resins, in: M. Gilbert (Ed.), Brydson's Plastics Materials (Eighth Edition), Butterworth-Heinemann2017, pp. 773-797.
[39] C.-J. Wang, C.-M. Chang, J.-M. Tseng, Epoxy acrylic resin experimental analysis of runaway reaction, Journal of Thermal Analysis and Calorimetry 138(4) (2019) 2839-2851.
[40] M.R. N, G. Babu, R. Saminathan, A.M. Babeer, H. H, A. Y.P, Experimental investigation on compression strength of EPOXY/PVC blend with different fibre glass reinforcements, Materials Today: Proceedings 49 (2022) 1650-1657.
[41] P.S. Chandel, N.K. Gupta, Y.K. Tyagi, K. Jha, Experimental Investigation of Water Absorptions and Charpy Test of Epoxy Composite Immersed in Different Aqueous Medium, in: A.K. Dubey, A. Sachdeva, M. Mehta (Eds.) Recent Trends in Industrial and Production Engineering, Springer Singapore, Singapore, 2022, pp. 79-92.
[42] F.-L. Jin, X. Li, S.-J. Park, Synthesis and application of epoxy resins: A review, Journal of Industrial and Engineering Chemistry 29 (2015) 1-11.
[43] L.C. Hollaway, A review of the present and future utilisation of FRP composites in the civil infrastructure with reference to their important in-service properties, Construction and Building Materials 24(12) (2010) 2419-2445.
[44] O. Büyüköztürk, M.J. Buehler, D. Lau, Lau, C. Tuakta, Structural solution using molecular dynamics: Fundamentals and a case study of epoxy-silica interface, International Journal of Solids and Structures 48(14–15) (2011) 2131-2140.
[45] T. Zhou, C. Wu, Y. Wang, A.P. Tomsia, M. Li, E. Saiz, S. Fang, R.H. Baughman, L. Jiang, Q. Cheng, Super-tough MXene-functionalized graphene sheets, Nature Communications 11(1) (2020) 2077.
[46] J.P. Johnston, B. Koo, N. Subramanian, A. Chattopadhyay, Modeling the molecular

structure of the carbon fiber/polymer interphase for multiscale analysis of composites, Composites Part B: Engineering 111 (2017) 27-36.
[47] L.-h. Tam, A. Zhou, C. Wu, Nanomechanical behavior of carbon fiber/epoxy interface in hygrothermal conditioning: A molecular dynamics study, Materials Today Communications 19 (2019) 495-505.
[48] X.Q. Wang, D. Lau, Atomistic investigation of GFRP composites under chloride environment, Advances in Structural Engineering (2020) 1369433220961749.
[49] Z. Wang, Q. Lv, S. Chen, C. Li, S. Sun, S. Hu, Effect of interfacial bonding on interphase properties in SiO2/epoxy nanocomposite: a molecular dynamics simulation study, ACS applied materials & interfaces 8(11) (2016) 7499-7508.
[50] S. Nouranian, C. Jang, T.E. Lacy, S.R. Gwaltney, H. Toghiani, C.U. Pittman, Molecular dynamics simulations of vinyl ester resin monomer interactions with a pristine vapor-grown carbon nanofiber and their implications for composite interphase formation, Carbon 49(10) (2011) 3219-3232.
[51] I.Y. Chang, J.K. Lees, Recent Development in Thermoplastic Composites: A Review of Matrix Systems and Processing Methods, Journal of Thermoplastic Composite Materials 1(3) (1988) 277-296.
[52] Y. Yan, J. Xu, H. Zhu, Y. Xu, C. Yang, Molecular dynamics simulation of the interface properties of continuous carbon fiber/ polyimide composites, Applied Surface Science 563 (2021) 150370.
[53] L. Pan, H. Guo, L. Zhong, M. Wang, X. Yuan, Influence of surface-modified glass fibers on interfacial properties of GF/PEEK composites using molecular dynamics, Computational Materials Science 188 (2021) 110216.
[54] J.L. Santiago García, M.I.L. Bastarrachea, M. de Jesús Aguilar Vega, Aromatic Polyamides Density from Molecular Dynamics Simulation, Macromolecular Symposia 325-326(1) (2013) 120-124.
[55] L.-h. Tam, A. Zhou, R. Zhang, C. Wu, Effect of hygrothermal environment on traction-separation behavior of carbon fiber/epoxy interface, Construction and Building Materials 220 (2019) 728-738.
[56] C. Wu, J. Jiang, L.-h. Tam, An atomistic study of creep deformation in fiber/matrix interface, ICCM22 2019: 22nd International Conference on Composite Materials, Australia: Melbourne, VIC, 2019, pp. 2526-2535.
[57] L.-h. Tam, J. Jiang, Z. Yu, J. Orr, C. Wu, Molecular dynamics investigation on the

interfacial shear creep between carbon fiber and epoxy matrix, Applied Surface Science 537 (2021) 148013.
[58] Accelrys Software Inc.: Materials Studio.
[59] L. Martínez, R. Andrade, E.G. Birgin, J.M. Martínez, PACKMOL: a package for building initial configurations for molecular dynamics simulations, Journal of computational chemistry 30(13) (2009) 2157-64.
[60] Y. Miyano, M. Nakada, Durability of fiber-reinforced polymers, John Wiley & Sons2017.
[61] L.-M. Zhou, J.-K. Kim, Y.-W. Mai, Micromechanical characterisation of fibre/matrix interfaces, Composites Science and Technology 48(1) (1993) 227-236.
[62] X. Li, X. Zhang, J. Chen, L. Huang, Y. Lv, Effect of marine environment on the mechanical properties degradation and long-term creep failure of CFRP, Materials Today Communications 31 (2022) 103834.
[63] M. Zhang, B. Jiang, C. Chen, D. Drummer, Z. Zhai, The Effect of Temperature and Strain Rate on the Interfacial Behavior of Glass Fiber Reinforced Polypropylene Composites: A Molecular Dynamics Study, Polymers 11(11) (2019) 1766.
[64] L.-h. Tam, L. He, C. Wu, Molecular dynamics study on the effect of salt environment on interfacial structure, stress, and adhesion of carbon fiber/epoxy interface, Composite Interfaces 26(2) (2018) 1-17.
[65] L.-h. Tam, C.L. Chow, D. Lau, Moisture effect on interfacial integrity of epoxy-bonded system: a hierarchical approach, Nanotechnology 29(2) (2017) 024001.
[66] J.M. Wernik, B.J. Cornwell-Mott, S.A. Meguid, Determination of the interfacial properties of carbon nanotube reinforced polymer composites using atomistic-based continuum model, International Journal of Solids and Structures 49(13) (2012) 1852-1863.
[67] F. Liu, N. Hu, H. Ning, Y. Liu, Y. Li, L. Wu, Molecular dynamics simulation on interfacial mechanical properties of polymer nanocomposites with wrinkled graphene, Computational Materials Science 108 (2015) 160-167.
[68] Z. Wei, R. Sinko, S. Keten, E. Luijten, Effect of surface modification on water adsorption and interfacial mechanics of cellulose nanocrystals, ACS applied materials & interfaces 10(9) (2018) 8349-8358.
[69] B. Li, J. Chen, Y. Lv, L. Huang, X. Zhang, Influence of Humidity on Fatigue Performance of CFRP: A Molecular Simulation, Polymers 13(1) (2020) 140.
[70] J.-K. Kim, C. Hu, R.S.C. Woo, M.-L. Sham, Moisture barrier characteristics of organoclay–epoxy nanocomposites, Composites Science and Technology 65(5) (2005) 805-

813.
[71] F. Vukovi, T.R. Walsh, Moisture Ingress at the Molecular Scale in Hygrothermal Aging of Fiber–Epoxy Interfaces, ACS Applied Materials and Interfaces 12(49) (2020) 55278-55289.
[72] R. Chahal, M.R. Raihan, K. Reifsnider, Y.T. Wu, Molecular Dynamics For The Prediction Of The Interface Dielectric & Mechanical Properties Of Carbon Fiber Epoxy Composites, American Society of Composites, 2018.
[73] N.L. Post, F. Riebel, A. Zhou, T. Keller, S.W. Case, J.J. Lesko, Investigation of 3D Moisture Diffusion Coefficients and Damage in a Pultruded E-glass/Polyester Structural Composite, Journal of Composite Materials 43(1) (2008) 75-96.
[74] Y. Xiao, G. Xian, Effects of moisture ingress on the bond between carbon fiber and epoxy resin investigated with molecular dynamics simulation, Polymer Composites 39(S4) (2017) E2074-E2083.
[75] X.Q. Wang, O. Büyüköztürk, C.K.Y. Leung, D. Lau, Atomistic prediction on the degradation of vinylester-based composite under chloride and elevated temperature, Composites Science and Technology 226 (2022) 109539.
[76] V.M. Karbhari, K. Ghosh, Comparative durability evaluation of ambient temperature cured externally bonded CFRP and GFRP composite systems for repair of bridges, Composites Part A: Applied Science and Manufacturing 40(9) (2009) 1353-1363.
[77] Z. Jia, T. Li, F.-p. Chiang, L. Wang, An experimental investigation of the temperature effect on the mechanics of carbon fiber reinforced polymer composites, Composites Science and Technology 154 (2018) 53-63.
[78] Y. Wang, J. Zhang, G. Fang, J. Zhang, Z. Zhou, S. Wang, Influence of temperature on the impact behavior of woven-ply carbon fiber reinforced thermoplastic composites, Composite Structures 185 (2018) 435-445.
[79] A.P. Thompson, H.M. Aktulga, R. Berger, D.S. Bolintineanu, W.M. Brown, P.S. Crozier, P.J. in 't Veld, A. Kohlmeyer, S.G. Moore, T.D. Nguyen, R. Shan, M.J. Stevens, J. Tranchida, C. Trott, S.J. Plimpton, LAMMPS - a flexible simulation tool for particle-based materials modeling at the atomic, meso, and continuum scales, Computer Physics Communications 271 (2022) 108171.
[80] B.R. Brooks, C.L. Brooks, 3rd, A.D. Mackerell, Jr., L. Nilsson, R.J. Petrella, B. Roux, Y. Won, G. Archontis, C. Bartels, S. Boresch, A. Caflisch, L. Caves, Q. Cui, A.R. Dinner, M. Feig, S. Fischer, J. Gao, M. Hodoscek, W. Im, K. Kuczera, T. Lazaridis, J. Ma, V. Ovchinnikov, E. Paci, R.W. Pastor, C.B. Post, J.Z. Pu, M. Schaefer, B. Tidor, R.M. Venable, H.L. Woodcock,

X. Wu, W. Yang, D.M. York, M. Karplus, CHARMM: the biomolecular simulation program, Journal of computational chemistry 30(10) (2009) 1545-614.
[81] JSOL CAE Solution Software Inc.: J-OCTA.
[82] H.J.C. Berendsen, D. van der Spoel, R. van Drunen, GROMACS: A message-passing parallel molecular dynamics implementation, Computer Physics Communications 91(1) (1995) 43-56.
[83] D.A. Case, T.E. Cheatham Iii, T. Darden, H. Gohlke, R. Luo, K.M. Merz Jr, A. Onufriev, C. Simmerling, B. Wang, R.J. Woods, The Amber biomolecular simulation programs, Journal of computational chemistry 26(16) (2005) 1668-1688.
[84] W. Humphrey, A. Dalke, K. Schulten, VMD: Visual molecular dynamics, Journal of Molecular Graphics 14(1) (1996) 33-38.
[85] OVITO GmbH Software Inc.: OVITO.
[86] K. Momma, F.J.J.o.A.C. Izumi, VESTA 3 for three-dimensional visualization of crystal, volumetric and morphology data, 44 (2011) 1272-1276.
[87] S.C. Chowdhury, R. Prosser, T.W. Sirk, R.M. Elder, J.W. Gillespie Jr., Glass fiber-epoxy interactions in the presence of silane: A molecular dynamics study, Applied Surface Science 542 (2020) 148738.
[88] J.P. Johnston, B. Koo, N. Subramanian, A. Chattopadhyay, Modeling the molecular structure of the carbon fiber/polymer interphase for multiscale analysis of composites, Composites Part B Engineering 111(FEB.) (2017) 27-36.
[89] K. Lin, T. Yu, Debonding simulation of fibre-matrix interfaces of FRP composites with reactive force field, Construction and Building Materials (2021) 125304.
[90] B. Arash, H.S. Park, T. Rabczuk, Tensile fracture behavior of short carbon nanotube reinforced polymer composites: A coarse-grained model, Composite Structures 134 (2015) 981-988.
[91] C.M. Hadden, B.D. Jensen, A. Bandyopadhyay, G.M. Odegard, A. Koo, R. Liang, Molecular modeling of EPON-862/graphite composites: Interfacial characteristics for multiple crosslink densities, Composites Science & Technology 76 (2013) 92-99.
[92] Q. Ji, R.J.M. Pellenq, K.J. Van Vliet, Comparison of computational water models for simulation of calcium–silicate–hydrate, Computational Materials Science 53(1) (2012) 234-240.
[93] P. Kowalczyk, P.A. Gauden, M. Wiśniewski, A.P. Terzyk, S. Furmaniak, A. Burian, K. Kaneko, A.V. Neimark, Atomic-scale molecular models of oxidized activated carbon fibre

nanoregions: Examining the effects of oxygen functionalities on wet formaldehyde adsorption, Carbon 165 (2020) 67-81.
[94] A. Dipak, G. Venkat, Reversal of Salt Concentration Dependencies of Salt and Water Diffusivities in Polymer Electrolyte Membranes, ACS Macro Letters 7(6) (2018) 739-744.
[95] S. Alessi, G. Pitarresi, G. Spadaro, Effect of hydrothermal ageing on the thermal and delamination fracture behaviour of CFRP composites, Composites Part B: Engineering 67 (2014) 145-153.
[96] X. Li, X. Zhang, J. Chen, L. Huang, Y. Lv, Effect of marine environment on the mechanical properties degradation and long-term creep failure of CFRP, Materials Today Communications 31 (2022) 103834.
[97] P.S. Shin, J.H. Kim, H.S. Park, Y.M. Baek, D.J. Kwon, K.L. Devries, J.M. Park, Evaluation of Thermally-Aged Carbon Fiber/Epoxy Composites using Acoustic Emission, Electrical Resistance and Thermogram, Composite Structures 196 (2018) 21-29.
[98] B. Zhang, S. Du, G. Qi, Y. Yu, A new approach to assessing carbon fiber/epoxy interfacial shear strength by tensile test of 45 degrees fiber bundle composites: Experiment, modeling and applicability, Composites Science & Technology 129 (2016) 214-221.
[99] E.V. Pisanova, S.F. Zhandarov, On the mechanism of failure in microcomposites consisting of single glass fibres in a thermoplastic matrix, Composites Science and Technology 57(8) (1997) 937-943.
[100] J.M. He, Y.D. Huang, Effect of silane-coupling agents on interfacial properties of CF/PI composites, 106(4) (2007) 2231-2237.
[101] J. Gou, B. Minaie, B. Wang, Z. Liang, C. Zhang, Computational and experimental study of interfacial bonding of single-walled nanotube reinforced composites, Computational Materials Science 31(3) (2004) 225-236.
[102] H. Wang, K. Jin, C. Wang, X. Guo, J. Tao, Effect of fiber surface functionalization on shear behavior at carbon fiber/epoxy interface through molecular dynamics analysis, Composites Part A: Applied Science and Manufacturing 126 (2019) 105611.
[103] L.-h. Tam, R. Wu, M.A.N. Minkeng, J. Jiang, A. Zhou, Understanding creep behavior of carbon fiber/epoxy interface via molecular dynamics simulation, In press. (2022).
[104] Z. Zhang, S.C. Gallo, X. Li, H. Dong, C.A. Charitidis, Evaluation of the creep behaviour of the carbon fibre in an unidirectional pultruded reinforced composite using nano-indentation technique, Polymer Testing 80 (2019) 106091.
[105] I. Yarovsky, Atomistic simulation of interfaces in materials: Theory and applications,

Australian Journal of Physics 50(2) (1997) 407-424.
[106] J. Koyanagi, N. Itano, M. Yamamoto, K. Mori, Y. Ishida, T. Bazhirov, Evaluation of the mechanical properties of carbon fiber/polymer resin interfaces by molecular simulation, Advanced Composite Materials 28(6) (2019) 639-652.
[107] A.P. Awasthi, D.C. Lagoudas, D.C. Hammerand, Modeling of graphene–polymer interfacial mechanical behavior using molecular dynamics, Modelling & Simulation in Materials Science & Engineering 17(1) (2009) 015002.
[108] R. Sinko, M. Vandamme, Z.P. Ba?Ant, S. Keten, Transient effects of drying creep in nanoporous solids: understanding the effects of nanoscale energy barriers, Proceedings. Mathematical, Physical, and Engineering Sciences 472(2191) (2016) 20160490.
[109] M.J. Adamson, Thermal expansion and swelling of cured epoxy resin used in graphite/epoxy composite materials, Journal of materials science 15(7) (1980) 1736-1745.
[110] M. Meng, H. Le, S. Grove, M. Jahir Rizvi, Moisture effects on the bending fatigue of laminated composites, Composite Structures 154 (2016) 49-60.
[111] B. Yu, Z. Jiang, J. Yang, Long-term moisture effects on the interfacial shear strength between surface treated carbon fiber and epoxy matrix, Composites Part A: Applied Science and Manufacturing 78 (2015) 311-317.
[112] J.C. Fogarty, H.M. Aktulga, A.Y. Grama, A.V. Duin, S.A. Pandit, A reactive molecular dynamics simulation of the silica-water interface, The Journal of Chemical Physics 132(17) (2010) 174704.
[113] I. Kafodya, G. Xian, L. Hui, Durability study of pultruded CFRP plates immersed in water and seawater under sustained bending: Water uptake and effects on the mechanical properties, Composites Part B: Engineering 70 (2015) 138-148.
[114] Z. Wang, X. Huang, G. Xian, H. Li, Effects of surface treatment of carbon fiber: Tensile property, surface characteristics, and bonding to epoxy, 37(10) (2016) 2921-2932.
[115] W. Chu, L. Wu, V.M. Karbhari, Durability evaluation of moderate temperature cured E-glass/vinylester systems, Composite Structures 66(1/-4) (2004) 367-376.
[116] Z. Zhai, B. Jiang, D. Drummer, Strain rate-dependent mechanical behavior of quasi-unidirectional E-glass fabric reinforced polypropylene composites under off-axis tensile loading, Polymer Testing 69 (2018) 276-285.
[117] L.-h. Tam, D. Lau, Effect of structural voids on mesoscale mechanics of epoxy-based materials, Coupled Systems Mechanics an International Journal 5(4) (2016) 355-369.
[118] D. Mamalis, C. Floreani, C.M. Ó Brádaigh, Influence of hygrothermal ageing on the

mechanical properties of unidirectional carbon fibre reinforced powder epoxy composites, Composites Part B: Engineering 225 (2021) 109281.
[119] R. Guo, G. Xian, C. Li, B. Hong, X. Huang, M. Xin, S. Huang, Water uptake and interfacial shear strength of carbon/glass fiber hybrid composite rods under hygrothermal environments: effects of hybrid modes, Polymer Degradation and Stability 193 (2021) 109723.
[120] R. Guo, G. Xian, F. Li, C. Li, B. Hong, Hygrothermal resistance of pultruded carbon, glass and carbon/glass hybrid fiber reinforced epoxy composites, Construction and Building Materials 315 (2022) 125710.

Table 2 Molecular simulation of glass fiber (GF)/matrix interfaces under environmental and loading conditions.

Author	Interface		Environment	Temperature (K)	Load	Forcefield	Mechanical properties		Adhesion properties			
	Fiber	Matrix					Tensile strength (MPa)	Shear strength (MPa)	Interaction energy ($mJ \cdot m^{-2}$)	Fracture energy ($mJ \cdot m^{-2}$)	Adhesion energy ($mJ \cdot m^{-2}$)	Energy barrier ($mJ \cdot m^{-2}$)
Lin et al. [36]	GF	Epoxy	Dry	300	Constant velocity	ReaxFF	286.2	/	/	/	/	/
Chowdhury et al. [87]	GF	Epoxy	Dry	300	Constant velocity	AMBER	340.0	320.0	/	/	/	/
	GF + SCA						1020.0 (+200%)	970.0 (+200%)	/	/	/	/
Zhang et al. [63]	GF	PP	Dry	250	Constant velocity	CVFF	145.0 (+12%)	/	/	14930.0 (+26%)	/	/
				298			130.0	/	/	11815.0	/	/
				363			117.0 (-10%)	/	/	10070.0 (-15%)	/	/
				403			113.1 (-13%)	/	/	8920.0 (-24%)	/	/
Pan et al. [53]	GF	PEEK	Dry	300	Constant velocity	COMPASS	/	40.3	312.6	/	/	/
	GF + SCA						/	55.7 (+28%)	440.9 (+41%)	/	/	/
Stoffels et al. [21]	GF	Epoxy	Dry	300	/	CHARMM	/	/	207.9	/	/	/
	GF + SCA						/	/	252.4 (+21%)	/	/	/
	GF		1 wt% moisture content			CHARMM; TIP3P	/	/	148.6 (-29%)	/	/	/
	GF + SCA						/	/	158.1 (-24%)	/	/	/

Higuchi et al. [24]	GF	Epoxy	Dry	300	Constant velocity	CHARMM	1380.0	/	80.6	/	/	/
			Addition of five water molecules			CHARMM; TIP3P	1080.0 (-22%)	/	62.9 (-22%)	/	/	/
			Addition of ten water molecules				952.2 (-31%)	/	50.8 (-37%)	/	/	/
Wang et al. [26, 45, 75]	GF	Epoxy	Dry	300	/	CVFF	/	/	973.0	/	/	/
				320			/	/	935.1 (-4%)	/	/	/
				340			/	/	913.6 (-6%)	/	/	/
				360			/	/	856.2 (-12%)	/	/	/
			Water immersion	300		CVFF; TIP3P	/	/	301.6 (-69%)	/	/	/
				320			/	/	293.2 (-70%)	/	/	/
				340			/	/	287.0 (-71%)	/	/	/
				360			/	/	283.2 (-71%)	/	/	/
			Saltwater immersion	300			/	/	243.3 (-75%)	/	/	/

The percentage in bracket represents the change of value compared with dry condition at RT, and "+" and "-" means an increase or a decrease respectively.

Table 3 Properties of carbon fiber/matrix interfaces under different environmental and loading conditions.

Author	Interface		Environment	Temperature (K)	Load	Forcefield	Mechanical properties		Adhesion properties			
	Fiber	Matrix					Tensile strength (MPa)	Shear strength (MPa)	Interaction energy ($mJ \cdot m^{-2}$)	Fracture energy ($mJ \cdot m^{-2}$)	Adhesion energy ($mJ \cdot m^{-2}$)	Energy barrier ($mJ \cdot m^{-2}$)
Johnston et al. [88]	CF	Epoxy	Dry	300	Constant velocity	MMFF	377.5	/	/	/	/	/
Yan et al. [52]	CF	PI	Dry	300	Constant velocity	PCFF	/	331.1	/	/	/	/
Wang et al. [102]	CF	Epoxy	Dry	300	Constant velocity	COMPASS	/	36.3	/	612.0	/	/
	CF + -COOH						/	51.2 (+41%)	/	875.2 (+43%)	/	/
Koyanagi et al. [22, 106]	CF	Epoxy	Dry	300	/	CVFF	/	/	151.0-174.0	/	/	/
Li et al. [37, 69]	CF	Epoxy	Dry	300	Cyclic load	CVFF	295.4	/	1300.2	/	/	/
			30 wt% moisture			CVFF; TIP3P	121.1 (-59%)	/	52.1 (-96%)	/	/	/
Chahal et al. [72]	CF	Epoxy	Dry	300	Constant velocity	ReaxFF	/	188.0	/	/	/	
			0.5 wt% moisture			ReaxFF; SPC	/	116.6 (-38%)	/	/	/	
Xiao et al. [74]	CF	Epoxy	Dry	300	/	CVFF	/	/	/	3.2	/	/
			Water immersion			CVFF; TIP4P	/	/	/	1.2 (-63%)	/	/

Tam et al. [17, 18, 47, 55-57, 64, 103]	CF	Epoxy	Dry	300	Constant velocity	CVFF	187.0	111.1	/	713.0	3.2	/
					Sustained load		44.84-45.64	28.02-28.82	/	/	/	4.9 (peeling); 4.0 (shearing)
				323	Constant velocity		162.9 (-13%)	78.0 (-30%)	/	634.6 (-11%)	3.1 (-13%)	/
			Water immersion	300		CVFF; TIP3P	113.3 (-40%)	77.8 (-30%)	/	270.4 (-62%)	1.0 (-70%)	/
				323			98.0 (-48%)	68.8 (-38%)	/	223.2 (-69%)	0.9 (-72%)	/
			Saltwater immersion	300			97.0 (-47%)	/	/	/	0.8 (-75%)	/
				323			84.0 (-55%)	/	/	/	0.7 (-78%)	/
Li et al. [96]	CF	Epoxy	Dry	298	Sustained load	CVFF	406.5	/	/	/	/	/
			4 wt% moisture	298		CVFF; TIP3P	302.6 (-26%)	/	/	/	/	/
				334			273.2 (-33%)	/	/	/	/	/
				354			255.1 (-37%)	/	/	/	/	/
			Saltwater immersion	298			297.6 (-27%)	/	/	/	/	/
				334			247.8 (-39%)	/	/	/	/	/
				354			247.7 (-39%)	/	/	/	/	/